UNITED KINGDOM • CHINA • MALAYSIA

Deciphering the role of NF-κB and STAT-1/3 in the pathology of a murine model of Lewy Body Dementia.

By Jack John Cooper, B.Sc. (Hons)

Student No: 14320266

ABSTRACT

This study was conducted to investigate and further understand the precise relationship between selected members of the transcription regulating families of both NF-kB and STAT in promoting neuroinflammation. This was attempted by measuring differences in the co-localisation of the selected proteins alongside the proliferative hypertrophy of astrocytes known as astrogliosis. Results were acquired using a previously generated 'neuronal-specific Ubiquitin proteasome pathway (UPP) -dysfunctional mouse model of Lewy Body Dementia'. Findings show a significant increase in astrogliosis within the model. Furthermore it was observed that STAT-1 and STAT-3 have time-dependant differences in protein expression. However, definitive altered pathway regulation differences were not observed, thus a robust definition of this relationship could not be established. NF-kB could not be consistently detected suggesting an absence or unimportance in the model. This absence also hints at a potential experimental flaw, due to the ubiquitous nature of NF-kB. Ultimately, the observations recorded in this study do not present a definitive means by which the UPP-dysfunction dependent inflammation of the CNS is increased by virtue of NF-kB nor STAT proteins.

Acknowledgments

The author wishes to express gratitude to the following:

Dr Bedford, L; Dr Layfield, R and Wilson, V; for providing supervision and aid in numerous topics pertaining to this paper.

Thanks for technical support and training are also given to the following: Lawler, K; Snary, A; Wesson, F; Rockliffe, A; Scott, D; Ducker, C and Rathbone, A.

Thanks are given to my friends and family, for both emotional and financial support- without either I would not have been able to complete this study.

Contents

Chapter 1: Introduction

Neuroinflammation is a hallmark of several neurodegenerative disorders (ND's), such as amyotrophic lateral sclerosis (ALS), Alzheimer's Disease (AD), (1) and Lewy Body Dementia. Neuroinflammation is defined as chronic CNS inflammation primarily mediated by constitutively 'activated' glial cells (2). Many signalling pathways cause the activation of reactive glial cells (gliosis), such as: The Janus kinase/signal transducer and activator of transcription 3 (JAK/STAT3) (3), Mitogen-Activated Protein Kinase (MAPK) (4) and Nuclear Factor kappa-light-chain-enhancer of activated B cells (NF-κB) pathways. The STAT proteins, along with canonical NF-κB (RelA/p50) play central roles in the inflammatory process, thus their mechanisms of action within neuroinflammation require further investigation (5). The means of investigating the role of p65 and STAT1/3 in neuroinflammation was conducted by utilising neuron-specific 26S proteasome depleted (knock-out) mice [Psmc1] developed previously (6). Due to the disruption of the 26S proteasome, subsequently intraneuronal UPP functionality is impaired. The majority of neuropathological inclusions of neurodegenerative diseases, such as Pale and Lewy bodies consistently contain ubiquitylated proteins, alluding to an impairment of the UPP. Furthermore, genetic evidence strengthens the suggested role that the dysfunction of the ubiquitin system has a direct impact on the pathology of these diseases. A notable example of this is the parkin gene. In the case of juvenile Parkinson's disease, the protein encoded by the parkin gene (ubiquitin protein ligase) is mutated, affecting individuals in an autosomal recessive manner (7). The UPP is fundamental for the maintenance of intracellular homeostasis, through numerous means of action. Not only is regulation achieved by controlling the levels of short-lived regulatory proteins, which are involved in the cell cycle, transcription, and DNA repair, but also by removing aberrant, toxic proteins and by-products (8, 9). UPP-mediated proteolysis is emerging as an integral component in regulating neurodevelopment, synaptic function, and plasticity and the survival of neurons (10). Reactive glial cells have been shown to have an increased p65 expression, as well as nuclear translocation during neuroinflammation on numerous occasions (11,12&13). Due to the importance and abundance of astrocytes and microglia in the neuroinflammatory response, the relationship between the UPS, NF-κB and STAT1/3 activation and the subsequent effect this has upon hallmarks of neuroinflammation will be the focus of this study. Previous studies show sustained microglial NF-κB activation decreased motor neuron (MN) survival rates (1, 5). 'Activated' reactive astrocytes also have a negative effect upon white matter, subsequently leading to reduced spatial memory retention (11, 13).

Although many studies have tried to evaluate which of the glial cell types acts as the driving force of neuroinflammation in their respective models, many have shown a high degree of crosstalk and initiation between astrocytes and microglia.

1.2 Glial cells and their role in neuronal development and maintenance.

Microglia and astrocytes are the most abundant cells within the CNS, and the basis of the CNS's immunological response. Individually, they each perform a myriad of roles in the maintenance and development of the CNS (15). Astrocytes are responsible for the maintenance of neuronal intracellular levels of glutathione (GSH) (16, 17). GSH is a major antioxidant, accounting for approximately 90% of available intracellular non-protein thiols. Intracellular GSH predominantly detoxifies and eliminates toxic Reactive Oxygen Species (ROS) molecules from cells. This elimination ensures the maintenance of a homeostatic redox status. This is achieved by reducing ROS's ability to induce oxidative stress, which is well known for leading to neuronal damage (18). Astrocytes also contribute to synaptic plasticity via the metabolic interaction they maintain with neurons. A key result of this association leads to the *de novo* synthesis of glutamate as well as G-aminobutyric acid (GABA). Both of molecules are crucial neurotransmitters, with a well-established involvement in long term potentiation, along with memory formation (19). Astrocytic regulation of synaptic transmission is crucial for preventing excitotoxicity (20). Excitotoxity of neural tissue leads to damage and a reduced sensitivity to stimuli. As such, preventing this form of toxicity is a major pillar in maintaining a healthy CNS. This is primarily achieved by the re-uptake of both neurotransmitters, coordinated by the glutamate aspartate transporter (GLAST) (21) and glutamate transporter 1 (GLT1) (22). The importance of these receptors for maintenance can be seen due to their high levels of protein expression, particularly localised within CNS on astrocytes. Further metabolic process, such as the release of growth factors (NGF, BDNF, and FGF-2) and TCA cycle intermediates (energy metabolism) are also responsible for the structural maintenance and regulation of neural tissue. Incidentally, the outdated notion of the CNS being an 'immunologically privileged', separated system is due to the formation of astrocytic processes into the blood-brain barrier (BBB) (23).

Microglia and macrophages are phagocytic cells that constitutively express several families of receptors, that when activated facilitate the removal of aged, necrotic tissues and toxic molecules from circulation within their surroundings (24, 25). The removal of noxious substrates and defective neuronal tissue is fundamental for the proper maintenance and development of the CNS. Despite microglia being predominantly phagocytic in nature, the glial cells do also produce a variety of neurotrophic factors that promote neurogenesis.

The seemingly dichotomous functions of microglia enables a diverse range of roles, particularly in coordinating the regulation of synaptic plasticity. Unsurprisingly microglia and astrocytes have many overlapping, synergistic roles. Furthermore, microglia also secrete numerous other trophic factors, such as basic fibroblast growth factors (FGF), nerve growth factor (NGF), and Insulin like growth factor 1 (IGF-1) (26). IGF-1 is particularly interesting, due to its secretion being shown to induce multipotent rat hippocampus-derived neural progenitor cells to differentiate into oligodendrocytes (20). This is a vital step in developing and maintaining the CNS, as oligodendrocytes are required for the myelination of neurons in the CNS, akin to Schwann cells in the PNS. The importance of myelination in the CNS is most clearly seen in patients with multiple sclerosis, (MS) a demyelinating disease that can cause motor/sensory disruptions (21, 22). Furthermore, IGF-1 has also been shown to protect immature oligodendrocytes from glutamate-mediated apoptosis (20). Microglia further support the maintenance of CNS functionality via the elimination of immature, faulty neurons resulting from aberrant differentiation and migration (27). This process requires the secretion of numerous factors / inflammatory mediators. Of particular note is the role reactive oxygen species (ROS) play in neurodegenerative development attributable to microglia (28). Due to the numerous functions of microglia briefly outlined, it is apparent that the glial cells have an intimate connection in shaping the synaptic network (synaptic pruning) of developing neurons to establish the mature CNS Circuit and maintain synaptic homeostasis (29,30,31&32). Finally, the release of neurotransmitters and neuropeptides by neurons promotes neuron-glia communications that further fine-tune the homeostatic regulation by microglia (33, 34). It is apparent that the establishment and maintenance of a healthy nervous system requires a substantial level of regulated utilisation of numerous microglial and astrocytic functions.

1.3 Neuroinflammation: from protection to destruction.

The process of neuroinflammation is characterised by the detection and response to noxious stimuli. Numerous signals induce an inflammatory response, In particular Reactive Oxygen Species (ROS) or the formation of faulty protein aggregates (35). The stimulation of glial cells by noxious stimuli (in response to a perceived threat to the CNS) leads to the subsequent release of proinflammatory molecules (cytokines) in numerous forms- chemokines, interleukins and tumour necrosis factors. These molecules subsequently ‘recruit’ glial cells to the site of inflammation in a protective manner (initially) via chemoattraction. However, if the cause of inflammation is unresolved, the continued accumulation of glial cells and release of cytokines becomes detrimental.

A critical result of this sustained, chronic inflammation is the proliferative hypertrophy of glial cells, known as gliosis. Whilst numerous forms of gliosis inevitably contribute in some manner to neuroinflammation, astrogliosis will be the predominant form investigated in this study (36).These reactive glial cells are perceived to be the primary cause of the detrimental results of neuroinflammation (37). Whilst this immunological response has been shown to be neuroprotective when initiated in response to a short-term infection or trauma, long term neuroinflammation has been linked to neurodegeneration via the formation of astrocytic scar/ lesions. The physiological changes associated with neuroinflammation are the result of sustained proinflammatory alteration of gene expression within astrocytes. This alteration of the transcriptome leads to the upregulation of toll-like receptors (38), and subsequently intracellular calcium levels. This has a myriad of effects, predominantly in relation to sustained astrocyte activation (furthering astrogliosis) (39). Interestingly, it was noted that astrocytes were found to be susceptible to oxidative stress in cultured human astrocytes caused by glutathione depletion, leading to the activation of SASP-associated inflammatory pathways, such as NF-κB and p38MAPK. This activation leads to the increased secretion of the cytokine IL-6 (40). Furthermore, another recent study of note found repeated lipopolysaccharide administration (a widely practiced technique used to mimic chronic inflammation) resulted in cultured BV2 microglial cells displaying numerous signs of senescence, such as enhanced SA-Bgal activity as well as senescence-associated heterochromatin foci (SAHF) (41).

1.3.1 Figure 1: Astrogliosis progression (36)

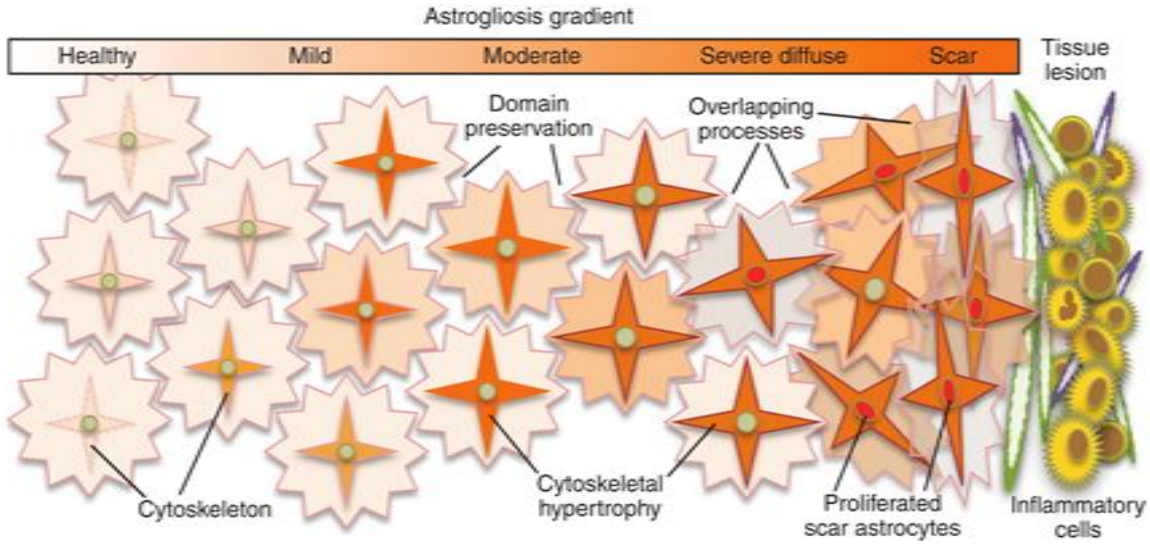

Figure Legend

Reactive astrogliosis is initiated and sustained by the release of proinflammatory cytokines. The unregulated inflammatory response within the CNS is the driving force behind neuroinflammation induced CNS degeneration. Chronic inflammation, which occurs over a period of many decades leads to adverse effects such as the destruction of functional, necessary neural tissue. This impacts the maintenance and functionality of the BBB along with a plethora of other detrimental outcomes. Another damaging effect of sustained inflammation is the development of astrocytic scars. The scars hinder normal neuronal regeneration mechanistically by causing domain overlaps, leading to a physical barrier preventing regrowth. Pinpointing the cause of prolonged CNS inflammation is difficult due to a wide range of stimuli and the many pathways that are involved in the subsequent response.

1.3.1 The numerable variables that lead to sustained Neuroinflammation

The continued inflammation leading to neurodegeneration progresses in a gradient dependent manner, reflecting the stark contrast between healthy and the disease inducing, aberrant functions of glial cells. Whilst it is known that the sustained reactive activation of both astrocytes and microglia contribute to inflammatory mediated neurodegeneration; it is not fully understood which cell type plays the major role. This is due to the interdependent activation of glial cells by each other, illustrated in Figure 2. Definitive instigators / factors that are responsible for the apparent physiological differences between healthy and neurodegenerative tissues have yet to be fully explored. It is well established that poor dietary and lifestyle habits are crucial in the maintenance of neuroinflammation (42). However, it is important to also consider that disruptions of normal immunological function of the brain as a result of genetic predispositions to ND's, such as inborn errors are also culpable. Epidemiological studies, alongside complementary data from animal models support this case; the exposure to pesticides and other environmental toxins, such as paraquat and MPTP, contribute to the development of PD neuropathology (43). This is due to the chronic overstimulation of glial cells and accumulation of ROS and inflammatory factors (especially cytokines) (43, 44). This suggest environmental exposure to toxins is capable of inducing senescence and an accompanying SASP. This makes distinguishing the contribution to neurodegeneration associated with both normal brain ageing and neurodegenerative disease much more difficult.

1.3.2 Figure 2: The Neuroinflammatory response, adapted from (45)

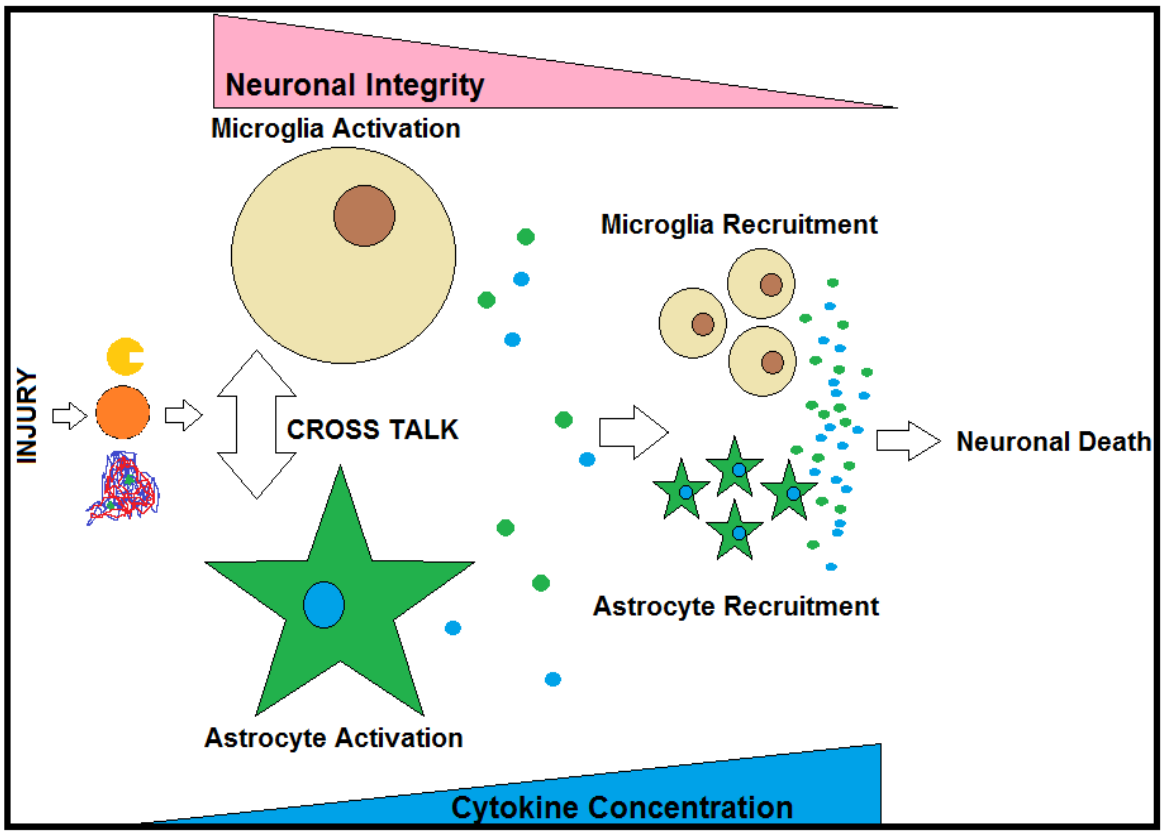

Figure Legend

When an injury or perceived threat is detected by the CNS immune cells, the reactive activation results in the transcription of numerous proinflammatory mediators. The accumulation of glial cells as the result of prolonged reactive activation strengthens the inflammatory response. Left unchecked, this will result in damage to neural tissue typically seen in neurodegenerative disorders due to sustained immunological attack.

1.3.3 Figure 3: The Ubiquitin Proteasome Pathway (UPP) and Neuroinflammation

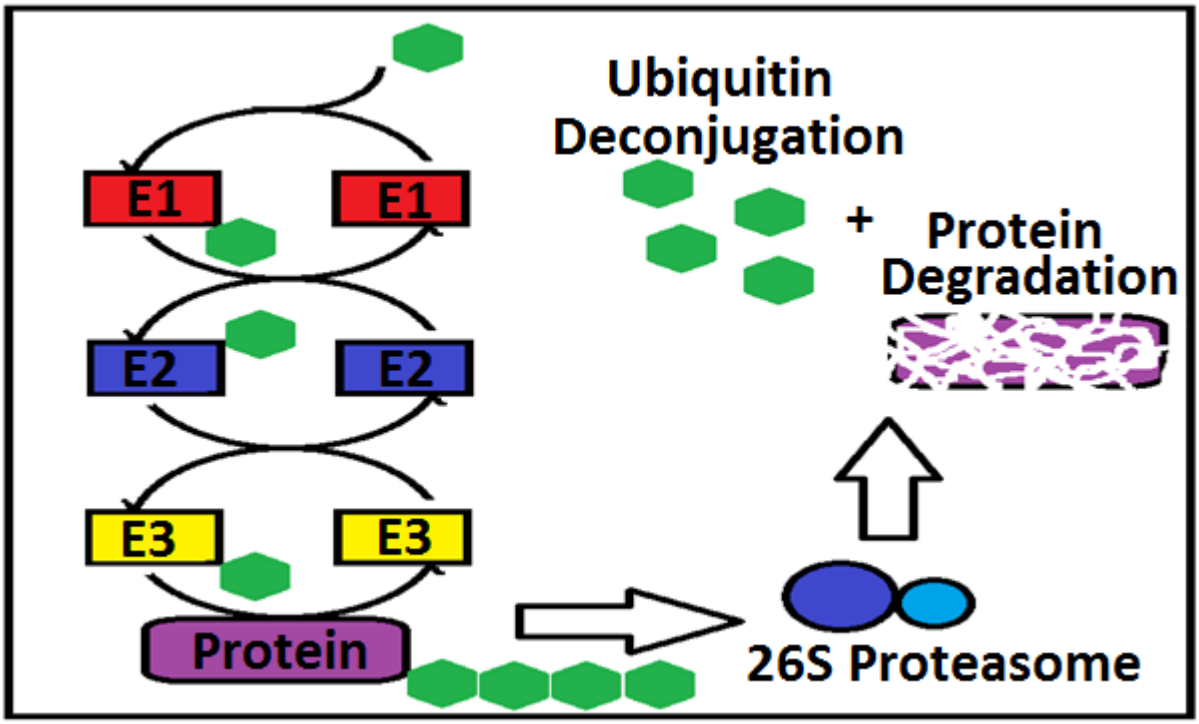

Figure Legend

Green Hexagon: Ubiquitin

The UPP consists of the directed actions of enzymes involved in forming chains of the polypeptide co-factor, Ubiquitin (Ub) from monomers. The enzymes involved, namely- **E1** (Ub-activating enzyme), **E2** (Ub-transporter) involved in catalysing the attachment of Ub via its C-terminal glycine residue to a lysine residue of the target protein via an amide bond. Lastly, **E3** (Ub-protein ligase) is able to recognize specific protein substrates and catalyse the transfer of activated Ub to the site of recognition. The poly-ubiquitination of proteins as a result of E1:3 marks them for degradation (46). This tagging and degradation process is the result of recognition by the 26S proteasome, a very large, varied-role protease complex that degrades ubiquitylated proteins to small peptides. Due to the onset of UPP dysfunction, the intra-neuronal accumulation of poly-ubiquinated proteins occurs post 2 and a half weeks in the mutant specimens used in this study (developed in lab previously, see Discussion 4.5 for further information). This model was used due to the known importance of ubiquitin rich neural inclusions in numerous ND pathologies. Specifically, Lewy-like inclusions and extensive neurodegeneration in the nigrostriatal pathway and forebrain regions were observed previously post the initiation of 26S proteasome subunit depletion.

1.3.4 The Sumoylation dependent pathway: Its role in post-translational Ubiquitination and the relationship it has to the UPP.

Ubiquitin and SUMO (small ubiquitin-like modifier) are the most prominent members of a conserved protein family of ubiquitin-like (UBL) post-translational modifiers. UBL proteins share an analogous, preserved ubiquitin fold. Furthermore, UBL proteins also share similar conjugating machinery comprised of specific activating and conjugating enzymes, termed E1 and E2. Substrate specificity is achieved by the activity of additional UBL ligases (E3), which form complexes with specific E2 proteins. The SUMO pathway functionally regulates a large variety of cellular processes, such as progression through the cell cycle, transcriptional regulation, DNA repair, stress responses, cancer and aging (47, 48).elucidating the precise molecular mechanisms underpinning the nature of SUMO modification in these processes is yet to be completed. With the exception of RanGAP1, only a minute fraction of a given protein pool is sumoylated at a certain point in time (47). SUMO modification alters protein function by affecting protein-protein interactions or subcellular localization. Until recently, SUMO and ubiquitin were thought to have opposing functions with Sumoylation hindering targeted protein degradation by occupying the same lysine residue that is required for their ubiquitination (49). A noteworthy and particularly relevant example leading to this concept was the modification of IκBα, an inhibitor of the transcriptional activator NF-κB (50). Upon activation of the inflammatory response pathway, IκBα is ubiquitylated and degraded by the proteasome releasing active NF-κB for nuclear transposition. However, IκBα can be sumoylated on the same lysine residue, this prevents its ubiquitination, preventing degradation and leading to stabilisation and maintenance of the protein (50). Based on this finding it has been suggested that SUMO modification of IκBα serves to inhibit the induction of NF-κB-dependent transcription. It seems in many cases, SUMO and ubiquitin can operate on the same lysine residue as a switch between different functional forms of a given protein. The role of Sumoylation was not investigated in this study. SUMOylation obvious and important role in the development of ubiquitin rich inclusions, has been seen previously in numerous studies (51). Despite this, results will be considered in light of UPP dysfunction. This UPP directed focus is due to the nature of model used, as well as the ubiquitous expression and pivotal role of the UPP in protein degradation in all cell types of interest to this study.

1.4 The Importance of NF-κB Activation.

NF-κB is a protein family responsible for the regulation of transcription for over 500 known genes (12). This study will focus on the role of RelA/p65-p50 canonical pathways role played in reactive astrogliosis and its relevance to the development of intraneuronal inclusions seen in the 26S proteasome depleted model. NF-κB activation has been shown on numerous occasions to play a significant role in neurodegeneration by way of glial activation in vivo/vitro. The activation of NF-κB is often responded to via the production and secretion of cytokines (7), capable of inducing numerous inflammatory responses. It has been shown on numerous occasions that the majority of the cytokines and chemokines produced via non-stimulated and activated astrocytes are direct targets of the NF-κB pathway. This suggests a central role of this factor in the proinflammatory (neurotoxic) and immunoregulatory (neuroprotective) actions of astrocytes in the CNS (52). NF-κB is well known to be involved in numerous other functions, related to: neuronal survival, differentiation, apoptosis, neurite outgrowth, and synaptic plasticity. The regulation of these functions has been seen to be significantly altered in AD pathologies. (53). The activation of astrocytes and microglia, by virtue of NF-κB via Aβ stimulation results in the production of the pro-inflammatory cytokines IL-1β, IL-6, iNOS, and TNFα (54). Interestingly, the basal expression of NF-κB is more concentrated within the CNS when compared to various peripheral tissues (55). Furthermore, it should be noted that multiple reports and studies suggest a form of constitutively activated NF-κB, predominantly found within glutamatergic neural tissue, such as the cerebral cortex. Other areas with considerable expression of NF-κB above the norm include the hippocampus (specifically granule cells + pyramidal neurons of CA1/3) (56). In a recent study in human and mouse astrocyte cultures it was found that astrocytes undergo cellular senescence in response to a variety of stressors. "Exposure to an oxidant (H_2O_2) or proteasome inhibitor, or replicative exhaustion all led to the development of characteristics of senescence, including growth arrest, an enlarged flattened morphology, SA-Bgal expression, increased expression of the cell-cycle inhibitors p21 and p16INK4a, and the development of senescence-associated heterochromatin foci (SAHF). Due in part to the ubiquity of miRNA-125b abundance in the brain it is perhaps not too surprising that miRNA-125b up-regulation has been shown to be involved, in part, in the down-regulated expression of an important family of brain-essential genes"(57).

1.4.1 NF-κB's various pathways and their involvement in neuroinflammation.

Despite the relatively young age of the field of neuroinflammation, a great deal of information has been gathered. In particular, the pivotal role that environmental factors play in the activation of numerous receptors involved in inflammatory coordination. The Toll like receptors are a well-known protein family intimately involved in inflammation. Previous research has shown that ethanol promotes TLR4 signalling in glial cells by triggering the induction of inflammatory mediators (NF-κB) and subsequent cell death, suggesting that the TLR4 response could be an important mechanism of ethanol-induced neuroinflammation (58). The researchers further observed astrogliosis and other stereotypical hallmarks of neuroinflammation, which were in no small part attributable to NF-κB activation. Furthermore, TLR4 has been shown more recently to be activated by fatty acids (59). However, the effects of microglial activation differ from reactive astrogliosis. This difference is attributable to microglia's predominant role as phagocytic 'cleaners. The importance of lifestyle factors in the development of inflammation has been strengthened by the observations of repeated use of 3, 4-methlylenedioxymethamphetamine, (MDMA) in relation to neurotoxicity. MDMA has been shown to significantly elevate NF-κB expression (60). The administration of the A2a-R agonist CGS following MDMA significantly elevated the NF-κB expression both at mRNA and protein levels. By contrast, administration of the A2a-R antagonist SCH resulted in a decrease in the NF-κB levels. The results of these studies may indicate the potential for a pre-emptive therapy for the prevention of NF-κB induced inflammation. Both canonical and non-canonical NF-κB activation has been shown as a result of amyloid beta (Aβ) (61) . However, it is still not clear which of the two activation types predominates the other in AD. It has been suggested that the differential NF-κB activation is related to the stage of the disease, however this hypothesis has yet to be further substantiated. In rats treated with Aβ1−42 oligomers, it was shown that COX-2, IL-1β, and TNFα were expressed in reactive astrocytes surrounding the Aβ-injection site and in nearby blood vessels, as well was found co-localization of NF-κB proteins with GFAP and COX-2 (62). In primary astrocytic and mixed astrocytic-neuronal cell cultures from rats, the use of minocycline, (an anti-inflammatory agent) reduced astrocytic inflammatory responses together with a decrease in neuronal loss, caspase-3 activation, and caspase3-truncated Tau species in neurons (63). Minocycline has been shown to inhibit the NF-κB signalling pathway in spinal rat astrocytes (64). Although an exaggerated neuroinflammatory response is observed in AD, an absolute suppression of the NF-κB signalling pathway would be undesirable and potentially cause further damage.

In APPswe/PS1dE9 transgenic mice, the suppression of NF-κB attenuated astrogliosis, especially in the hippocampus and cortex of the tested animals. However, this was couple with an increased amount of Aβ1−42. This suggests a role of astrocytic-mediated clearance of Aβ in neuroinflammatory pathologies (65). Furthermore, the clinical evidence for the use of non-steroidal anti-inflammatory drugs (NSAIDS) in AD patients has not proven beneficial.

***1.4.2 Figure 4: Activation of the Canonical NF-κB Pathway adapted from* (66)**

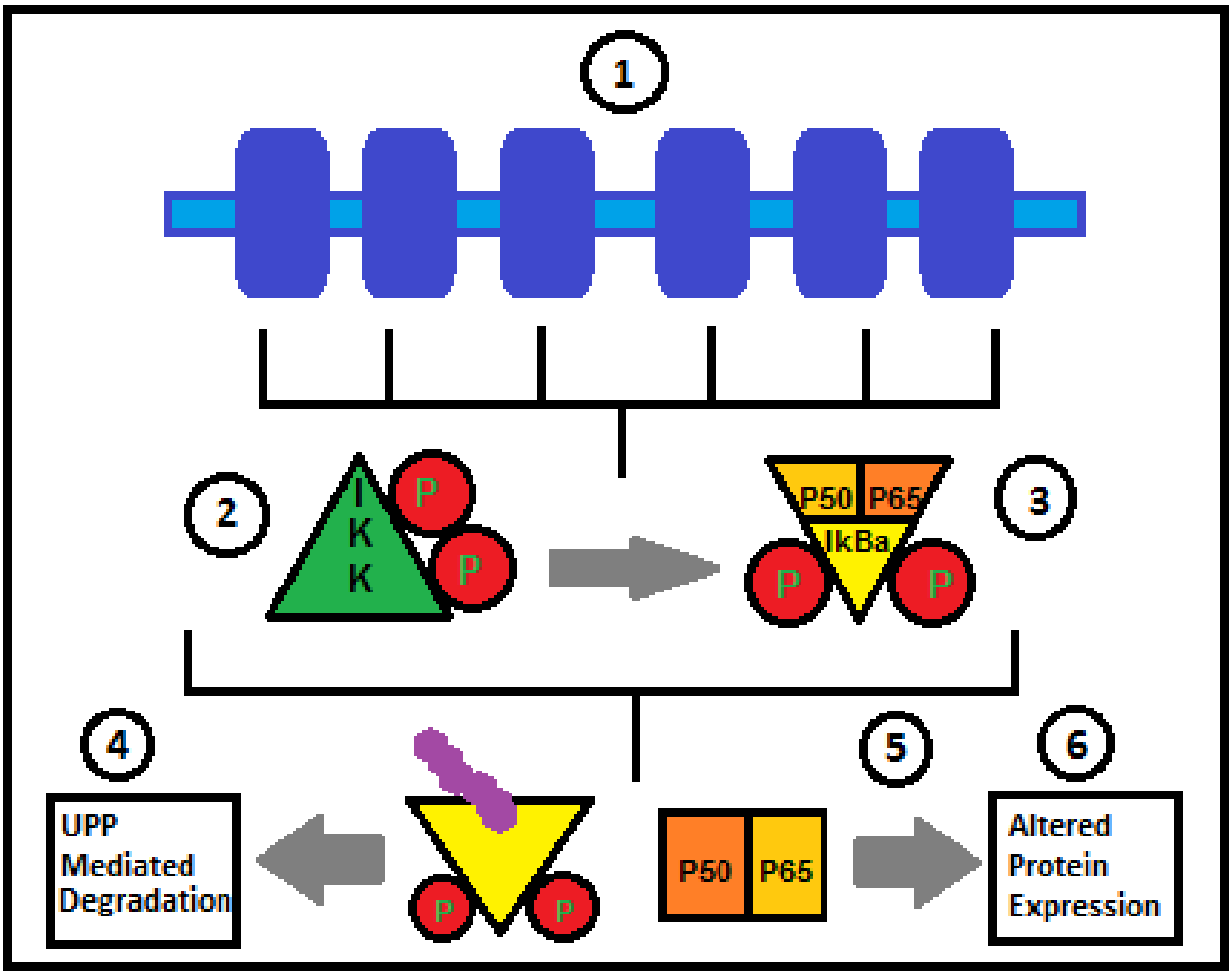

Figure Legend

(Detection - 1): The canonical NF-κB pathway is activated via pro-inflammatory signals, predominantly via cytokines, PAMPs and some DAMPs. (**Coordination - 2):** Upon cellular exposure and detection of inflammatory agents, extra/intracellular receptors coordinate the activation of the IKK-γ-associated kinase complexes by utilizing numerous proteins involved in ubiquitin chain formation. IKK-β is activated by phosphorylation at Ser_{177} and Ser_{181} via receptor coordinated kinases (67). (**Activation - 3):** Once canonical IKK is activated, phosphorylation via transfer from IKK-β allows ubiquitination to commence.

This process is needed for IκBα to separate from the p65-p50 heterodimer. With the IκB degraded, cytosolic bound p65-p50 heterodimer is now free for transport into the nucleus. (**UPP Degradation - 4):** The phosphorylation of IκBα on the N-terminal serines (Ser32/36) allows for the recruitment of the E3 ubiquitin ligase SCF/βTRCP. In conjunction with E1 and E2 ubiquitin-related enzymes, ubiquitination of IκBα targets it for degradation via the 26S proteasome (68). (**Transcription - 5):** The NF-κB heterodimer coordinates along with the aid of endogenous nuclear proteins at κB sites based on the composition of the 'binding' site created by dimerization. This leads to the transcription of the target protein, IκBα may also be produced as a means of negative feedback regulation. (**Targeted Protein Synthesis - 6):** The transcribed protein, encoded within the produced RNA is synthesized- this protein is the cell's means of response to the detection of inflammatory mediators.

1.4.3 NF-κB Protein Classes: Structural Functions & Familial Homology.

The ability of the NF-κB pathway to modulate the expression of numerous immune related genes is a result of several key structural elements. These elements are found in all members of the family (69). This familial homology and combinational variance (by the formation of hetero/homodimers) between Class 1 and Class 2 Rel/NF-κB proteins provides a high degree of versatility in targeted gene regulation (70). The intra-protein location of the RelA-p50 heterodimer's key structural elements can be seen in Figure 4.

1.4.4 Figure 5: Structure of p50 + RelA (p65) monomers

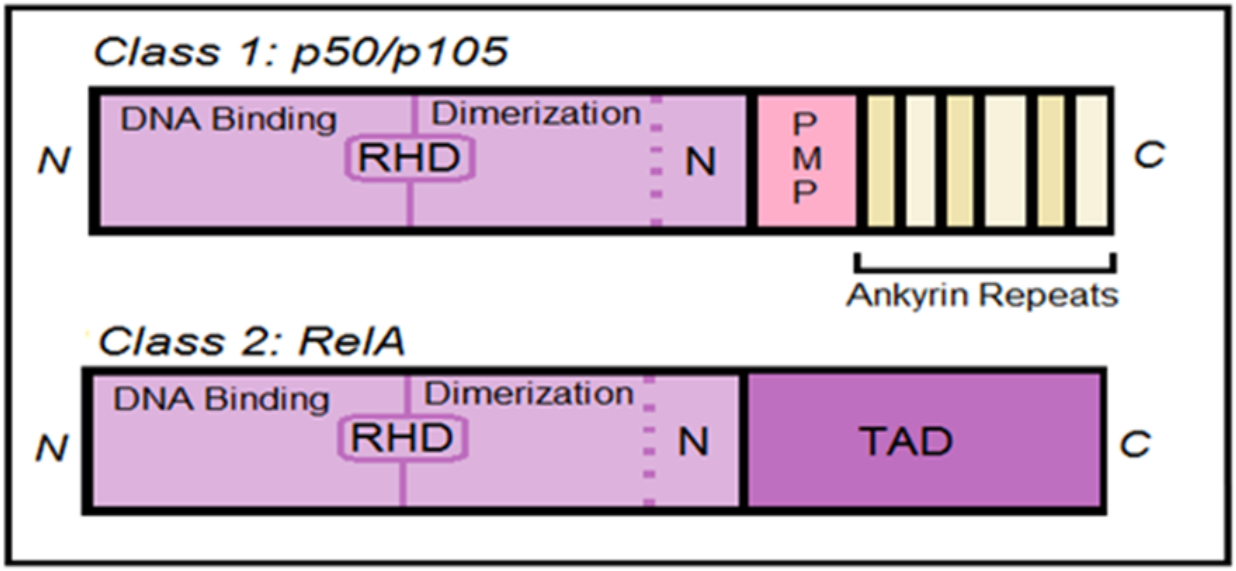

Figure Legend

NF-κB proteins can be sub-divided into two classes. **Class 1** includes proteins p105/100; these proteins are characterised by long C-terminal domains, with 6-7 ankyrin repeats. These repeats inhibit functionality until proteasome mediated proteolysis occurs at the required site (PMP). This limited proteolysis results in a smaller, functional, NF-κB protein. (p105 → p50). Once PMP has occurred, dimerization between class 1 and class 2 NF-κB proteins can commence (61). **Class 2,** which contains RelA (p65), contains C-terminal transcription activation domains; these are responsible for the initiation of transcription. Once activation and dimerization has occurred, Rel/NF-κB dimers bind to specific kB sites (9-10 base pair DNA sites). This binding leads to an upregulated expression of the targeted gene (71). On top of the already presented regulatory control structurally ingrained into both classes of NFkB proteins, there is further control imposed by proteins within the Inhibitors of kappa-B Kinase (IKK) family, discussed in further detail below.

1.4.5 Modulation of NF-κB (RelA/p50) activity by IκB kinase.

IκB kinase is a crucial regulatory enzyme complex closely involved in the activation of the canonical NF-κB pathway (72). The enzyme complex's immobilisation of NF-κB heterodimers within the cytoplasm is fundamental to its regulatory function. (73). Structurally, the IκB kinase is a trimeric protein complex comprised from subunits IKK-α, IKK-β and IKK-γ (Nemo). IKK-α along with IKK-β act as the repressors of dimeric proteins in NF-κB family, such as RelA/p50. The final non-catalytic subunit of the IKK complex is a crucial subunit, regulating the actions of IKK-α / β. IKK-γ self-regulates the complex via interactions within a domain contained within the amino-terminus. Furthermore, From residue 47 through to 120, this domain is responsible for inhibitory interaction with the kinase subunits (74). The formation of asymmetrical four helical bundles is the mechanism of inhibition. This is achieved via amino acids 44 to 111 NEMO) binding to the amino acids 701 to746 of the IKK-β subunit.

1.4.6 Figure 6: Key structural regions of IKK-β + IKK-α

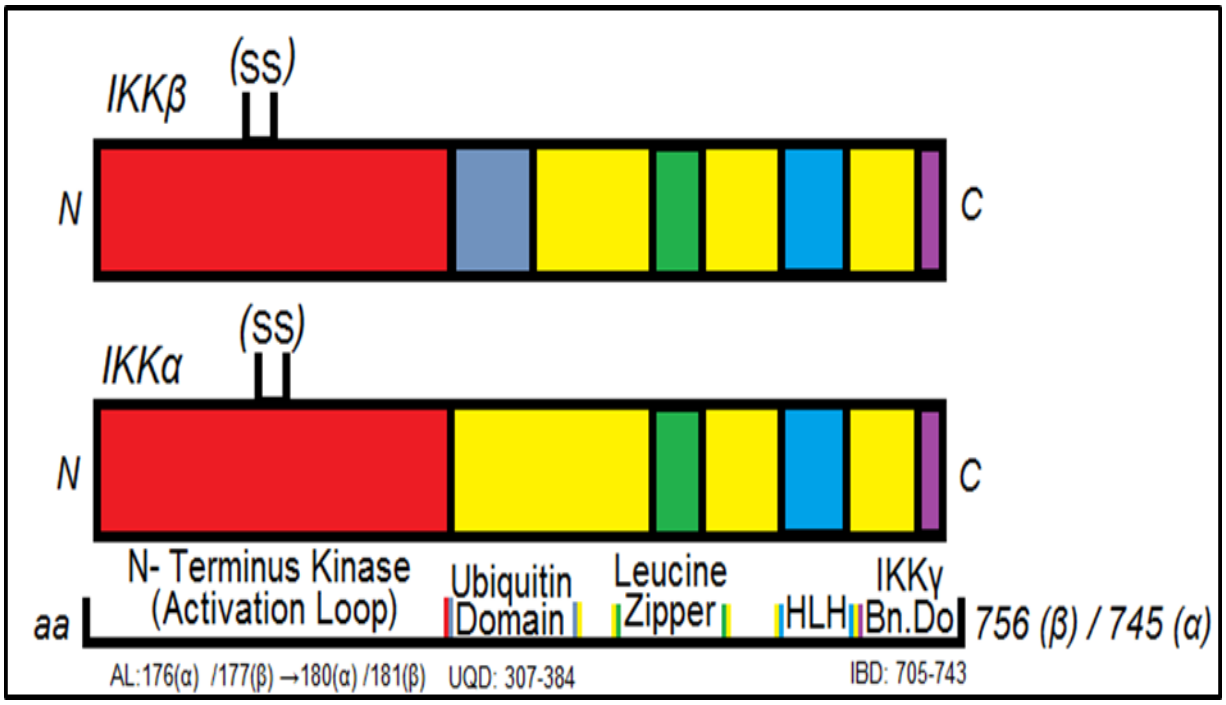

Figure Legend

IKKa and IKKb share a strong structural homology, of around 50% sequence identity. Similarities between the subunits include an N-terminal kinase domain (AL: Activation Loop. This is responsible for coordinating phosphorylation, in essence acting as an on/off switch. This is achieved by the phosphorylation of Serine 177,181 for IKKb (75), and Serine 176,180 for IKKa . This phosphorylation could potentially lead to a conformational change. This change regulates the activation of p65/p50 by modulating the sequestering capabilities of the 'catalytic' subunits of the IKK complex. Another protein domain essential to the functionality of the inhibitory complex include the helix-loop-helix (HLH) which further regulates IKK N-terminal kinase activity (72). The role of the leucine zipper found in both repressor subunits is not conclusively known; it is believed to aid in the dimerization process between IKKa and IKKb (76). Despite obvious similarities, IKKb ultimately is the key component of the IKK complex's role in coordinating the inhibition of NFkB dimers involved in the canonical pathway. This is due to its ubiquitin targeted proteolysis. This process is required to release the NFkB heterodimer for nuclear translocation. IKKb's structure contains an ubiquitin-like domain with unknown functionality (UQD: Ubiquitin like Domain). Experimental data has yet to reveal conclusively which interactions are mediated by IKKb's ubiquitin binding domain and others that have been tested (77).

1.5 The Importance of STAT1/3 activation.

The signal transducer and activator of transcription (STAT) proteins are a familial group of intracellular transcription factors (78). They are fundamental constituents in a wide range of roles responsible for the mediation of cellular immunity, proliferation and differentiation. These roles are initiated and coordinated by various means, however they are primarily activated by membrane receptor-associated Janus kinases (JAK) in response to cytokine detection. Gene knockout studies have showed that STAT proteins are involved in the development and function of the immune system and play a role in maintaining immune tolerance and tumour surveillance. Forced activation of JAK-STAT signalling leads to precocious astrogliogenesis, and inhibition of this pathway blocks astrocyte differentiation. These observations suggest that autoregulation of the JAK-STAT pathway controls the onset of astrogliogenesis.

1.6 STAT Protein Regulation.

It was initially observed that STAT proteins were latent cytoplasmic transcription factors, requiring phosphorylation (as seen in the JAK-STAT pathway) for nuclear importation (79). Once in the nucleus the activated STAT dimers can bind to consensus DNA-recognition motifs, called gamma-activated sites (GAS), in the promoters of cytokine-inducible genes, resulting in transcriptional activation. It has since been observed that phosphorylation is not a definitive prerequisite for transcriptional regulation by STAT family members. Studies on STATs 1 and 3 and 5 have demonstrated that unphosphorylated STATs shuttle between the cytoplasm and the nucleus in the absence of cytokine activation (80). while non-phosphorylated STAT proteins constantly shuttle between the cytoplasm and nucleus, the phosphorylated STAT protein is retained in the nucleus and is only released upon dephosphorylation by nuclear phosphatases, the case being the same for STAT 3 (81). Therefore, it can be said that nuclear retention, not translocation, of the active phosphorylated STAT protein is the important condition favouring cytokine-induced STAT activation. Furthermore, specific serine phosphorylation occurs at Serine 727 in response to IL-6-type cytokines, and Serine 708 is phosphorylated in response to IFNs. Phosphorylation is not the only means of regulating STAT protein activities. Depending on the protein in question, regulation can take place in a few ways. For STAT 1, post translational modification is a fundamental regulatory process. For example, de/acetylation affects IFN-induced tyrosine phosphorylation, and subsequently regulates specific gene / protein regulation. Furthermore, methylation of STAT1 on Arginine 31 also regulates STAT-1's functional capabilities.

Conversely, SUMOylation of STAT-1 on Lysine 703 by PIAS1 inhibits activation, this resolves in nuclear dephosphorylation and subsequently modulates STAT-1's DNA binding activity. STAT-3 is regulated via similar means as STAT-1. The de/acetylation of Lysine 685 by acetyltransferase p300 is involved in the regulation of growth and glucose metabolism. This modification is able to directly affect phosphorylation at Serine 727. This is because STAT-3 undergoes phosphorylation by pyruvate kinase M2, responsible for promoting cell proliferation in response to alterations in glucose metabolism. Regulated modifications are able to produce structural changes enabling a greater diversity in the roles STAT 1/ 3 are able to play. For example, the formation of C-terminally truncated STAT3 β and γ isoforms, is achieved by alternative splicing and proteolytic processing, respectively (85).

1.6.1 Figure 7: Activation of the JAK-STAT Pathway.

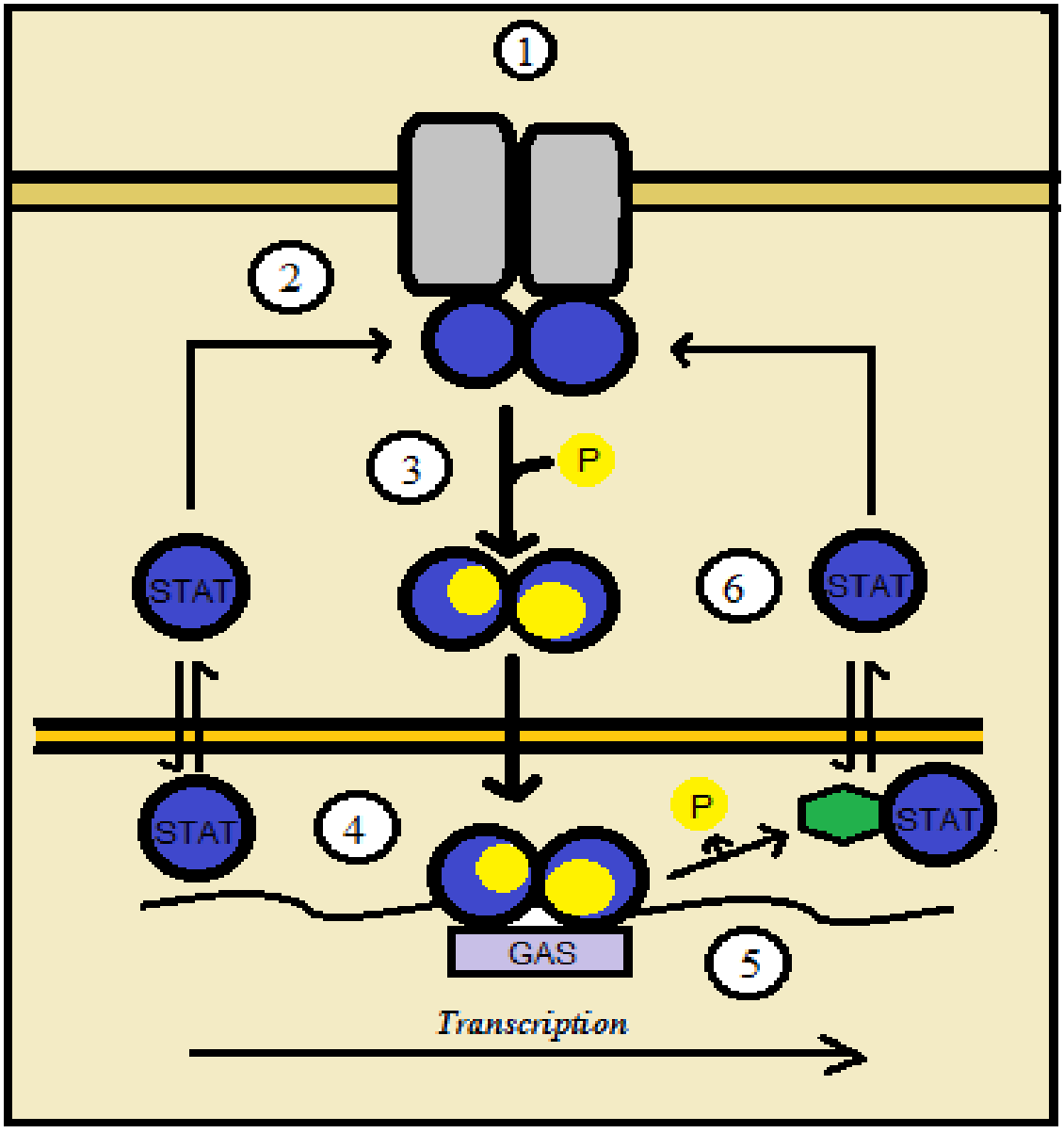

Figure Legend

(Detection - 1): Stimuli detection induces the activation of latent cytoplasmic JAK kinases. (**Initiation - 2):** This leads to the docking and subsequently, tyrosine phosphorylation of latent monomeric or N-domain-mediated dimeric STAT proteins. (**Activation – 3)**: This enables the formation of the catalytically active SH2-domain-mediated homodimers of STAT proteins (82). **(Nuclear Importation and Transcription – 4)**: The phosphorylated STAT dimers are actively transported to the nucleus via metabolic energy, utilising the importin α/β and RanGDP complex. Once Nuclear translocation is complete, the active STAT dimers bind to the promoters of genes containing the consensus recognition motif (**GAS motif**: TTC-XXX-GAA) and initiate transcription of these target genes. STAT familial structure allows them to bind to targeted DNA as either dimers or as N-domain-mediated tetramers (83). (**Deactivation and Halting Transcription – 5):** The active STAT protein(s) are released from DNA upon dephosphorylation by nuclear phosphatases. This is induced by a reduction/ withdrawal in cytokine recognition. The now inactivated protein is then actively exported out of the nucleus to the cytoplasm by the exportin Crm-1/RanGTP complex. Monomeric STAT proteins can also passively shuttle between the cytoplasm and the nucleus via carrier-free diffusion through nuclear pores facilitated by the interaction with nucleoporins (84).

1.4.2 STAT proteins: Structural Functions & Familial Homology.

The ability of the STAT family proteins to regulate numerous pathways and subsequent protein expression is the result of several key structural elements. These are found in all members of the family; this familial homology and combinational variance (by the formation of hetero/homodimers) between the isoforms provides a huge capacity for regulation. The intra-protein location of the STAT Family proteins' key structural elements can be seen in Figure 6.

1.6.2 Figure 8: Activation of the JAK-STAT Pathway. Adapted from (79)**.**

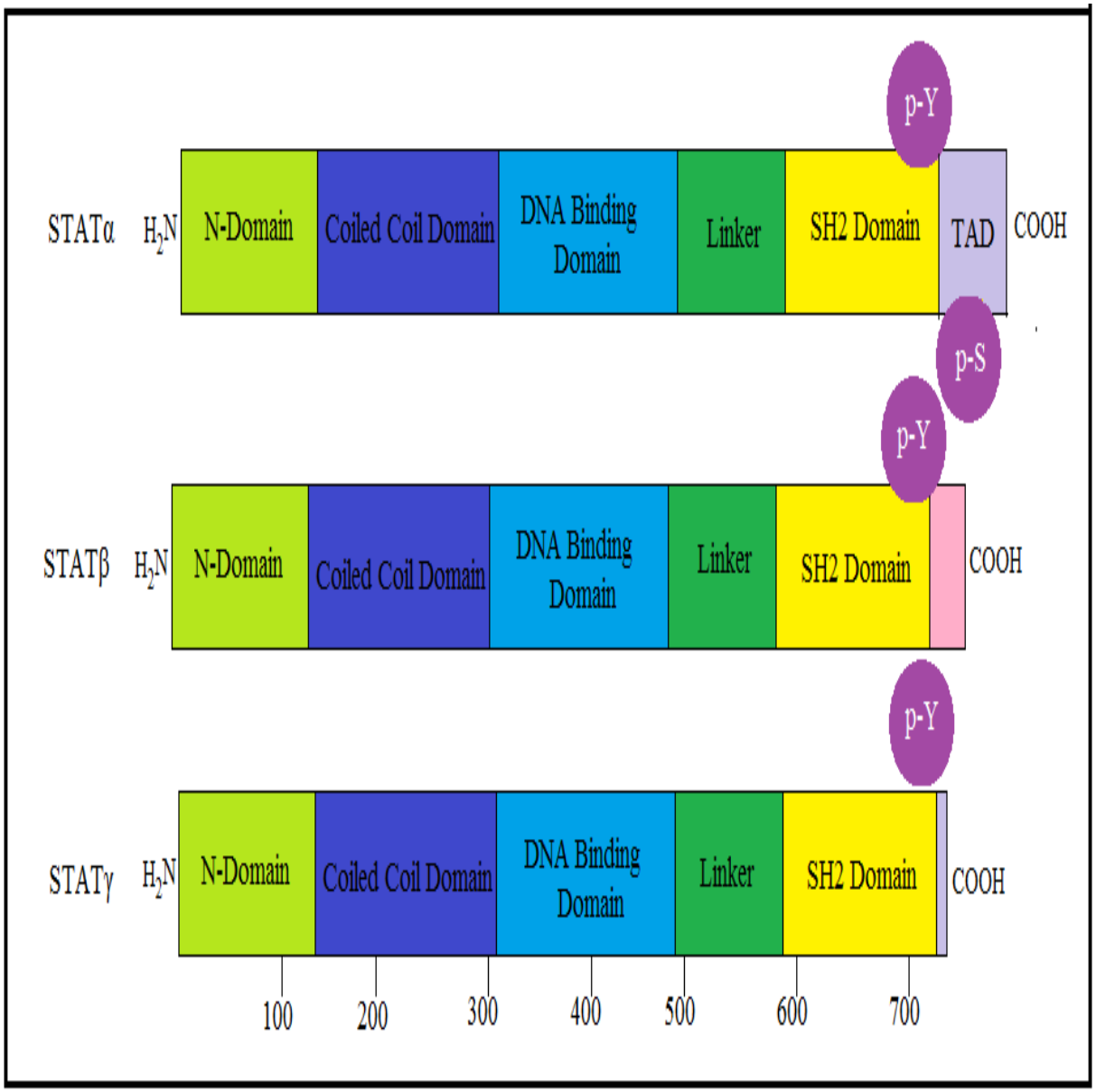

Figure Legend

All STAT proteins share a common molecular structure, they are further organized via distinct functional domains. The N-domain is involved in inter-protein interactions between adjacent STAT dimers on DNA, facilitating the formation of STAT tetramers. Additionally, the N-domain is also involved in the formation of dimers between non-phosphorylated STAT monomers. This is crucial for receptor-mediated activation and nuclear translocation of certain STAT proteins. Furthermore, interactions with STAT cofactors, which positively or negatively modulate their transcriptional activity, occurs via the N-domain. Cofactors also modulate activity with interaction with the coiled-coil domain and the carboxy-terminal transactivation domain (TAD).

The conserved serine residue (p-S), which is phosphorylated upon cytokine stimulation and is important for maximal transcriptional activation, is located within the transactivation domain. In addition to the full-length form (STATα), STAT proteins can also be present as C-terminally truncated forms generated by alternative splicing (STATβ) or by proteolytic processing (STATγ). The C-termini of STATβ proteins differs from the corresponding STATα protein not only by being truncated, but also by having additional amino acids inserted as a result of the splicing event (79, 90).

1.6.3 Modulation of STAT activity by phosphatases.

Phosphorylation of receptors and Janus kinases, are counteracted by phosphatases. For example, the SH2 domain contains the tyrosine phosphatases SHP-1 (PTPN6) and SHP-2. These are recruited to pTyr bearing SH2 recognition motifs in cytoplasmic receptor domains (85). Additional regulation occurs using SOCS (suppressors of cytokine signalling) and PIAS proteins (protein inhibitors of activated STAT), which are both components of negative feedback loops, acting as inhibitors of JAKs or STATs or directing them to protein degradation pathways (86). The expression of SOCS proteins is strongly induced by STAT-mediated gene regulation (87). SOCS can directly bind to JAKs or to the cytoplasmic domains of cytokine receptors, where they inhibit JAK binding and activity or the recruitment of STATs. Furthermore, SOCS proteins are also involved in the degradation of JAKs and STATs through the ubiquitin-proteasome pathway (88). Another protein connecting STATs to ubiquination and subsequent degradation is SLIM, which acts as an ubiquitin E3 ligase, particularly targeting STAT1 and STAT4. SLIM was also shown to inhibit STAT tyrosine phosphorylation. PIAS proteins are constitutively expressed, their suppression of STAT function relies on blockade of the STATs' DNA binding sites, or by functioning as ligases to subject STATs to SUMOylation and to funnel them into the SUMO-mediated degradation pathway (89). The small ubiquitin-related modifier (SUMO) is an interesting, versatile cellular tool used to modulate a protein's function. SUMO modification is a reversible process analogous to ubiquitination. The consecutive actions of E1, E2 and E3 enzymes catalyse the attachment of SUMO to target proteins, while deconjugation is promoted by SUMO specific proteases. Contrary to the long-standing assumption that SUMO has no role in proteolytic targeting and rather acts as an antagonist of ubiquitin in some cases, it has recently been discovered that sumoylation itself can function as a secondary signal mediating ubiquitin-dependent degradation by the proteasome.

The implication of SUMO in ubiquitination was the result of discovering a novel family of RING finger ubiquitin ligases, which bear SUMO interaction motifs, suggesting the ubiquitin system exerts a degree of control upon SUMO modified proteins.

1.8 Aims and Objectives

This study was an interdisciplinary undertaking, focusing on the pre-established connection between neuroinflammation, and subsequent neurodegenerative disorders. This project included two 'candidate' transcription factors known to be closely involved in neuroinflammation, the NF-κB and STAT families. Through the observation of changes in expression and localisation of these proteins, knowledge of essential signalling pathways in the murine model of LBD will be uncovered. This is a fundamental process for continued advancements in knowledge for both the previously generated murine LBD model and further aids the development of neurodegenerative disorders treatment as a whole. In order to provide a richer understanding of the topic at hand, both a quantitative and qualitative approach were utilised in this study. Due to the functional decline of the UPS, neuronal homeostasis is disrupted by the accumulation of polyubiquinated proteins (6), such as IKB. This disruption leads to the development of ubiquitin rich inclusions, a hallmark of age related neurodegeneration and activation of the neuroinflammatory response (91). Glial cells, such as astrocytes are the foundation of the CNS immune system. Due to the abundance of astrocytes and their importance in regulating neuron excitability and synaptogenesis (15), astrocytic inflammatory regulation was the focus of this undertaking.

1.8.1 Key experimental aims for project

The chief aims of this investigation will be:

1. To measure cellular sub localisation and activation of p65 and STAT-1/3 in relation to astrogliosis. It is expected that there will be a marked increase in expression and occurrence of protein nuclear translocation in the psmc KO samples versus the wild type controls due to the functional disruption of neuron-UPP. It is assumed that there will be an age dependant concentration increase in all candidate proteins alongside an increased frequency in nuclear translocation.

2. Nuclear translocation in non-astroglial cells, within the context of inflammation will be considered, however astroglial nuclear import will be the main focus. With this in mind, it is expected that there will be an astroglial (nuclear) predominance when investigating protein localisation and activation differences between the chosen model and control samples. Furthermore, another avenue of investigation is to determine if p65 and STAT-1/3 contribute to the development of intraneuronal inclusions as a potential alternative mechanism of inducing neuroinflammation irrespective of astroglial specific activation.

3. The disruption of target protein- inhibitor interactions will be briefly touched upon as well. Specifically, the concentration and localisation differences of Iκβα will be measured. The inhibition of p65 by Iκβα is due to it masking the nuclear localisation sequence, preventing translocation. Therefore, activation of p65 relies upon degradation of its inhibitor (Iκβα). This is canonically achieved by the ubiquitin proteasome system (UPS), which is considerably disrupted in the selected model samples. Thus, there is a natural inclination to suggest a marked cell specific increase in the nuclear translocation of p65 will be accompanied with a decreased co-localisation / expression of Iκβα.

Chapter 2: Materials and Methods

2.1 Mice: The provision of samples, which were produced in the laboratory previously was the starting point for this study. Generation of conditional 26S proteasome-deleted mice has been described in detail (see discussion, 4.5). Appropriate littermate mice were used as controls (Psmc1fl/fl;CaMKIIα-Wt and Psmc1fl/wt;CaMKIIα-Wt). All procedures were carried out previously by Dr Bedford and/or Lawler, K under personal and project licences granted by the UK Home Office in accordance with the ***Animals (Scientific Procedures) Act 1986*** and with ethical approval from the University of Nottingham Ethical Review Committee.

2.1.1 Materials

2.1.2 Primary Antibodies

Antibody	Company	Target	Dilution
SC-8008.	• Santa Cruz. • Biotechnology. • GeneTex.	**p65**	1:1000 **(WB)** 1:100 **(IHC)**
SC-136548. #3033.	• Santa Cruz. • Biotechnology. • Cell Signalling.	**p-p65**	1:1000 **(WB)** 1:100-1:50 **(IHC)**
GTX110521. SC-1643.	• GeneTex. • Santa Cruz. Biotechnology.	**Ικβα**	1:1000 **(WB)**
GTX632427	• GeneTex	**IBA-1**	1:200 **(IHC)**
G8795.	• Sigma Aldrich.	**GFAP**	1:5000 **(WB)** 1:400 **(IHC/IF)**
D1K9Y.	• Cell Signalling.	**STAT-1**	1:1000 **(WB)** 1:200 **(IHC/IF)**
58D6.	• Cell Signalling.	**p-STAT 1**	1:1000 **(WB)**
D1A5.	• Cell Signalling.	**STAT 3**	1:1000 **(WB)** 1:100 **(IF)**

2.2 Western immunodetection analysis.

2.2.1 Total homogenate sample preparation.

Microdissected brain regions from genotyped specimens were homogenized on ice in 50 mM Tris, pH 7.4, 175 mM NaCl, and 5 mM EDTA. Prepared samples were given to be used in this study (see appendices, 1). Stock volumes of samples were maintained at -80 C. Samples were thawed, mixed and kept on ice in preparation for use/loading. Protein estimation used the Bio-Rad (Bradford) protein assay kit, using a BSA concentration gradient for reference. Results were recorded and processed using Excel.

2.2.2 Sodium dodecyl sulphate polyacrylamide-gel electrophoresis (SDS-PAGE)

Samples were subjected to SDS-PAGE, with the resolving gel acrylamide concentration used ranging from 10-12%. This was prepared in house using Buffer B, 0.1% SDS, polyacrylamide, AMPS and TEMED and cast into pre-assembled cassettes (see appendices 11). This prepared gel was overlaid with a water saturated butanol solution, ensuring a straighter boundary between the resolving and stacking gel. The resolving gel was left to polymerise for a minimum of 30 minutes. Subsequently, the water-butanol solution was removed via deionised water (d H_2O). Once the now exposed surface of the polymerised resolving gel had dried, the stacking gel (see appendices, 11) was poured above the resolving gel. This was followed quickly by the insertion of well forming combs. The stacking gel was allowed to polymerise and set for a minimum of 30 minutes. After this, the comb was delicately removed to prevent damage to the formed wells. Any unpolymerized stacking gel solution was removed using d H_2O, and the gels were loaded into cassettes in preparation for sample loading. Electrophoresis occurred in the Mini-PROTEAN® Tetra Vertical Electrophoresis Cell, which was assembled and prepared accordingly. The running buffer used was prepared in house (See appendices, 11) and loaded into the cell system. This was followed by loading of samples into the preformed wells. The power supply settings were set as follows: 250 V 135 mA. Electrophoresis was performed until the blue dye loaded with the samples reached the bottom of the cassettes. This took approximately 1 hour to 1 and a half hours. Post protein separation, gel-bound proteins were transferred overnight to a prepared nitrocellulose membrane, ensuring bubbles of no contact between the gel and the membrane did not remain. Transfer was achieved using the Trans-Blot® Cell system, this was run using in house transfer buffer. Successful transfer was tested using the reversible copper stain method described in 2.2.2.

2.2.2 Copper staining method.

Membrane-bound proteins were visualised by first washing with TBS-Tween for 5 minutes, followed by copper staining for 5 minutes. This process is repeated once more, leading to distinctive blue banding, a result of copper-protein interactions. This indicates that successful transfer has occurred, along with the absence of any unknown abnormalities inspected for as well.

2.2.3 Immunodetection.

The prepared nitrocellulose membrane was blocked for at least 1 hour in the appropriate blocking medium (Marvel or BSA). This is to aid the prevention of undesired antibody-protein binding sites. Primary antibody incubation occurred post blocking and 3 times 5-minute washes in TBS-Tween. Incubation occurred for at least 1 hour at room temperature, however predominately occurred overnight at 4 C. The secondary antibody used for recognition by the LI-COR Odyssey® Infrared Imaging System, was the IRDye® 800CW Mouse/Rabbit IgG (1:5000). Images were processed and recorded using the Image Studio™ software suite. Samples were normalised to GAPDH, a housekeeping protein expressed ubiquitously, results are presented as a fold change of the control, described in more detail below.

2.3 Histological analysis

For light microscopy, samples were obtained from previously perfusion-fixed mice, using 4% paraformaldehyde in 0.1 M phosphate buffer, pH 7.4. Specimen brains were embedded in paraffin wax and sectioned (5 m) using in-house protocols.

2.3.1 Brightfield Microscopy

Morphological examination used Haematoxylin [Harris] and Eosin staining. Immunohistochemistry using DAB staining, was performed as directed in Vector Laboratories M.O.M Immunodetection [GFAP (Sigma)] or Vectastain Elite Rabbit IgG. ABC kits used either 0.01 M citrate or 10 mM EDTA buffer containing 0.05% Tween-20 pH 6/8.5 for antigen retrieval and appropriately conjugated secondary antibodies. The technique used was developed in lab previously (see appendices, 4). This technique was used as a means of preliminary qualitative analysis. Due to the limitations of DAB staining for quantification, other techniques were utilised to directly measure differences in protein concentration and localisation.

2.3.2 Immunofluorescent microscopy

Immunofluorescence is used due to the techniques ability to show the sub-cellular localisation of proteins with greater clarity for the observer. This is achieved using Fluorescent-conjugated antibodies that have emissions from differing wave lengths. This allows a variety of sub-cellular 'colouring' as a means of localisation. The technique used was developed in lab previously (see appendices, 6) Imagining was achieved using the Olympus BX51 microscope and camera. Image processing utilised the computer program ImageJ.

2.4 Statistical analysis

Data analysis for Western and Immunofluorescent results used two-tailed unpaired Welch's analysis with an unequal variance. The threshold for statistical significance (alpha) was set to 0.05. Standard deviation was also calculated and presented alongside significant findings where appropriate. Data analysis was achieved using Microsoft Excel.

Chapter 3: Neuroinflammation hallmarks- GFAP and IBA1.

Measuring the changes in GFAP and IBA-1 were chosen to as a means of following the development of neuroinflammation in samples. Qualitative assessment utilised DAB immunohistochemistry to approximated differences between WT and KO samples at various time points. General observation indicate an increased localisation and expression of both Astrocytic (GFAP) and microglial (IBA-1) cells. Astrocytic processes appear to be larger and more widely spread with a high degree of overlap in KO samples. There appears to be an age related increase at 6 Wks. for DAB but not fluorescent staining. Microglial cells appear to undergo physiological changes, with an increased cell size observed in KO samples as well (See 3.1.1 Fig 7). Furthermore, Immunofluorescent imaging of GFAP was also used as a means of measuring expression changes.

3.1 Figure 6 Wk. and 4 Wk. GFAP IHC analysis (WT/KO) (n=3 for each image shown)

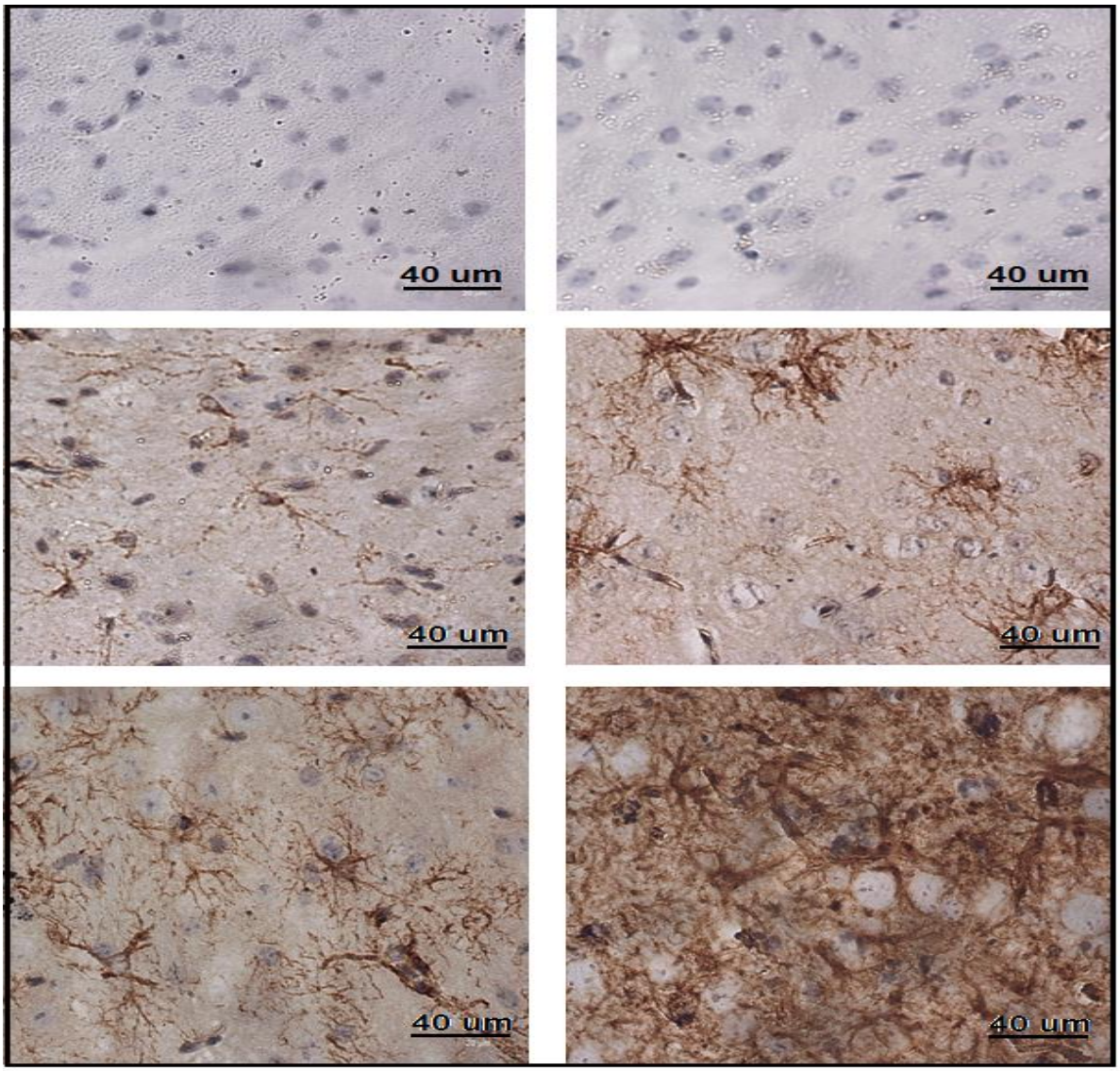

Figure Legend

GFAP expression and localisation (measurement of astrocyte reactivity) was recorded in coronal tissue sectioning samples (A/D negative control). As expected, a greater GFAP expression was observed in KO (B, D) samples. Furthermore, overall expression is increased comparatively in 6 (A-C) vs 4 (D-F) Wk. samples. Images were obtained at x 40 / 0.9 magnification using Axiovision software.

3.1.1 Figure 6 Wk. WT and KO IBA-1 IHC analysis (n=1)

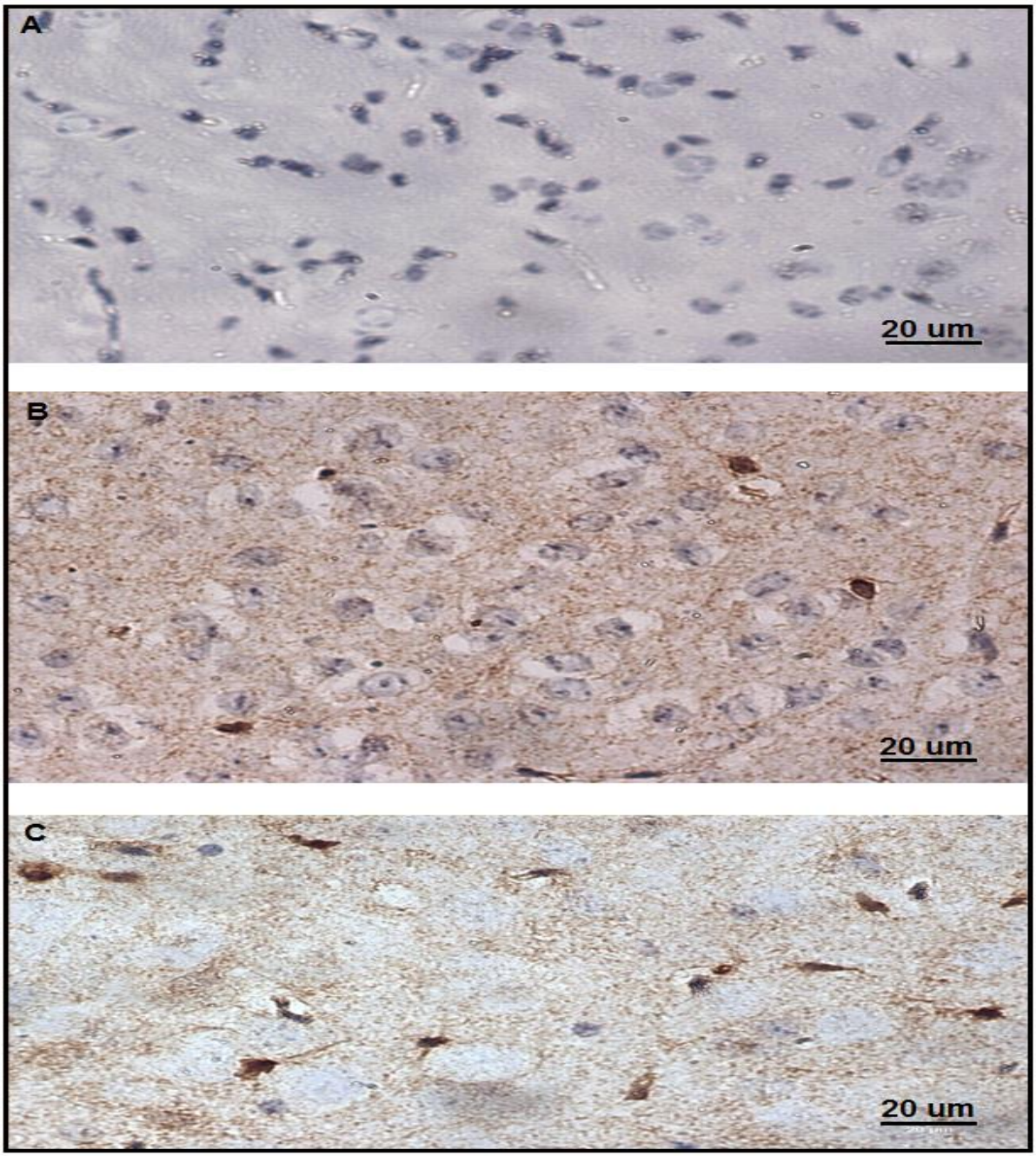

Figure Legend

IBA-1 expression and localisation was measured in microglia found in coronal tissue sectioning samples (Negative control: A). as expected, a greater IBA-1 expression was observed in the KO (C) sample. Furthermore, physiological differences between WT (A) and KO microglia suggest that a phagocytic phenotype is presented in KO samples. Images were obtained at x 40 / 0.9 magnification using Axiovision software.

3.2 Figure 4 Wk. vs 6 Wk. GFAP Area (%) in WT/KO (WT: n=4, KO:n=3)

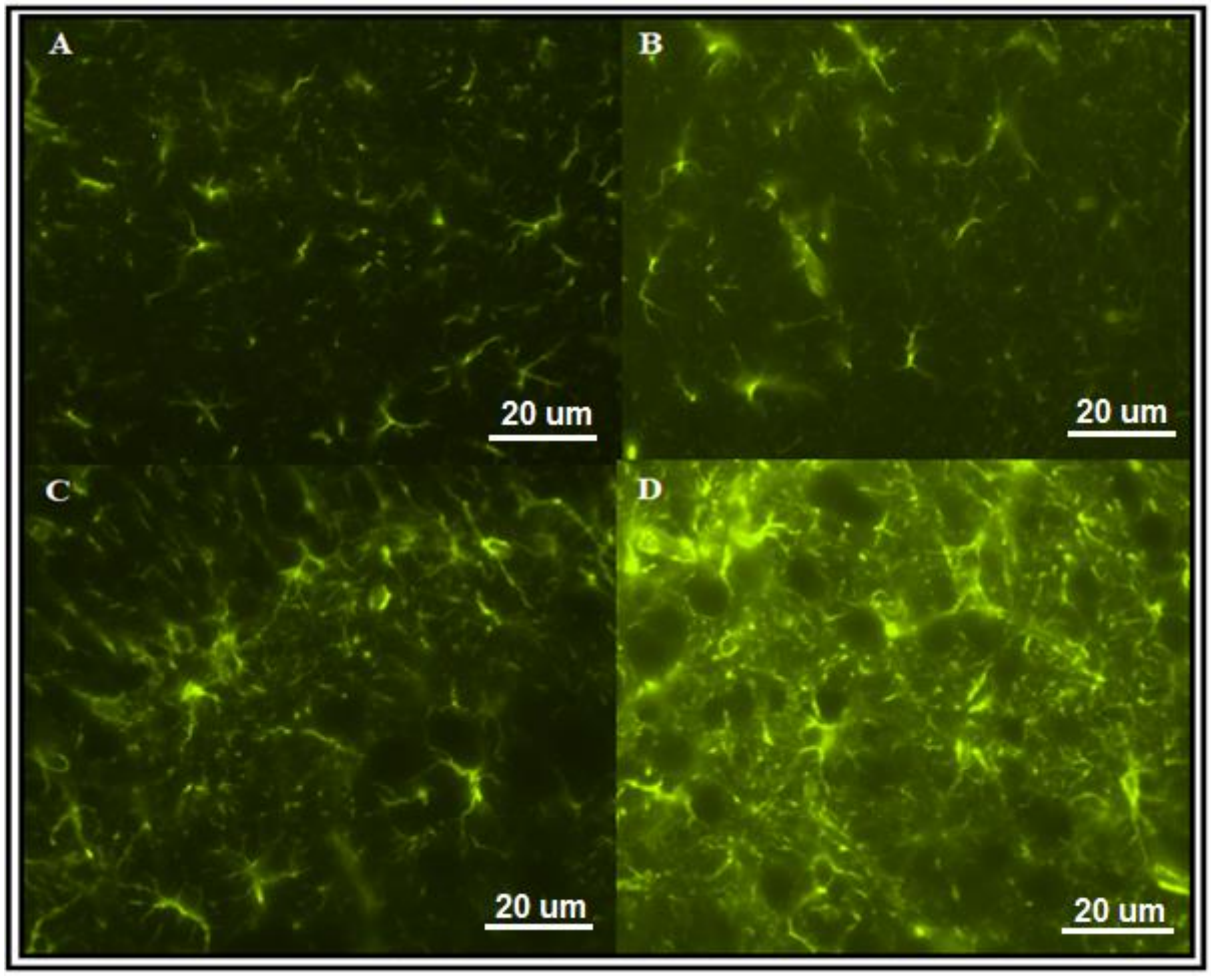

Figure Legend

GFAP expression and localisation was measured in coronal tissue sectioning samples. As expected, a greater GFAP expression was observed in KO (C, D) samples. Images were obtained at x 40 / 0.9 magnification using Axiovision software.

3.2.1 Figure differences in Total Area (%) of GFAP expression for 4 WK vs 6WK WT/KO samples.

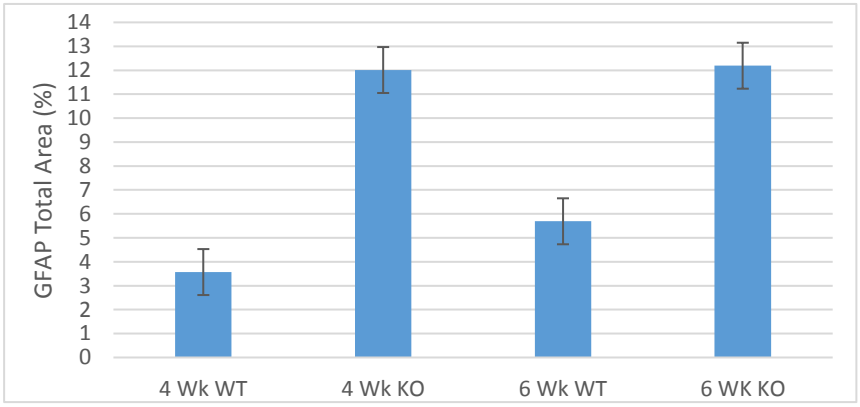

Standard Deviation
4 Wk. WT: 1.04
4 Wk. KO: 0.96
6 Wk. WT: 0.86
6 Wk. KO: 1.00

Area differences between 4 Wk. and 6 Wk. WT samples were found to be statistically significant. The differences in GFAP expression at 4 Wks. for WT.KO was found to be the result of the UPP dysfunction (p= 0.00002). This was not the case for the differences seen between 6 Wk. samples.

3.3 Summary of GFAP and IBA-1 results

GFAP, a measure of astrocytic reactivity was significantly elevated in KO samples. No differences were seen at 4 and 6 weeks. IBA-1 was found to be increased as well, however further testing is required to elucidate the significance of this singular result.

Chapter 3: P65 & Iκβα Results

3.4 P65 & Iκβα Western Blot analysis

Western Analysis was used to measure the protein expression of p65 and Iκβα in samples acquired from 4, 5&6 Weeks knock-out (KO) models and compared to Wild Type (WT) controls. Comparison of non/phosphorylated p65 utilised primarily Western blot (WB) analysis and DAB double staining immunohistochemistry. WB analysis proved to be inadequate in detecting quantifiable differences between the KO and WT samples for both forms of p65. Despite inconclusive results, p65 nuclear translocation was observed at 5 weeks in nuclear extraction samples (Fig. 1), hinting at activation. However, this was not observed in further nuclear samples (not shown). P65 was also detected in 6 Week cell homogenate samples (Fig.1), its presence was not seen in other non-nuclear samples at 4&6 weeks (not shown). The difference in expression of Iκβα between WT and KO was determined as non-significant, although was decreased at 4 weeks vs 6 (Fig.2).

3.4.1 Figure p65 in 5 Wk. Nuclear extraction samples vs 6 Wk. Total homogenate WT+KO samples. (n=1)

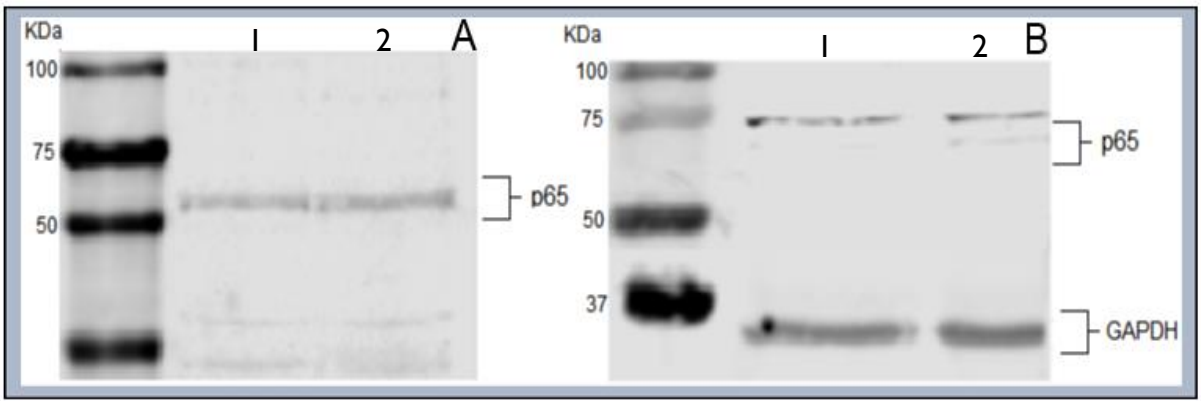

Figure Legend

Nuclear extraction samples (A, 1-2) show p65 was detected (no statistical difference). Cell homogenate samples (B, 1-2) showed faint detection of p65 in both WT and KO. Due to the signal difference and sensitivity of Odyssey©, GAPDH and p65 banding were measured separately.

3.4.2 Figure 2: IκBα in 6 Wk. vs 4 Wk. WT+ KO Total homogenate samples. (n=4)

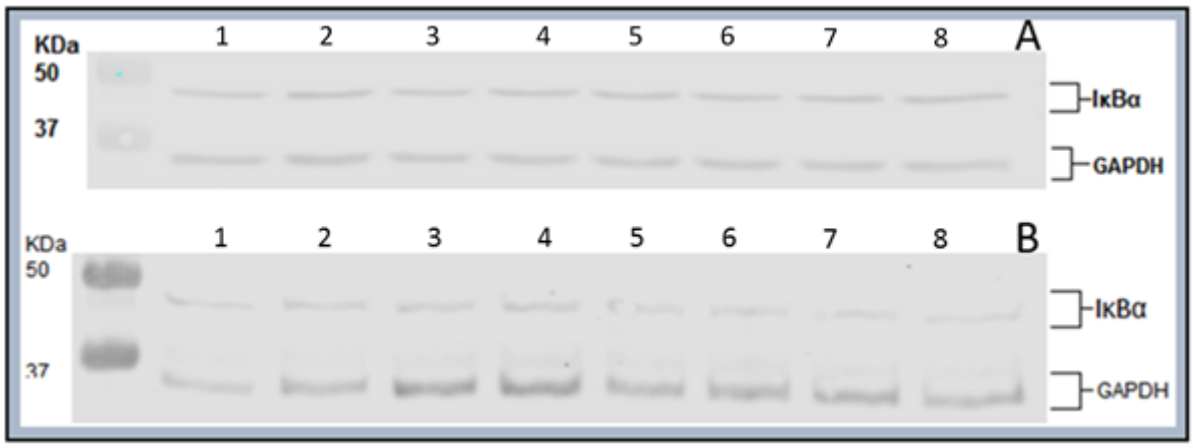

Figure Legend

6 Wk. samples showed no difference in expression between WT (A, 1-4) and KO (A, 5-8). 4 Wk. samples (B, 1-8) showed similar results as A. Also, B shows an overall reduced 'visual' expression when compared to A.

3.5 P65 Immunohistochemical analysis

Despite the lack of western results, analysis of p-/p65 localisation was measured in WT and KO 4&6 Wks. paraffin embedded perfusion fixed samples, sliced accordingly (5 µm). This was done on a preliminary basis to determine whether further investigation with p65 would prove fruitful. Glial p65 nuclear localisation was predominantly absent. Determining activation could not be achieved, due to no observable differences in localisation between p-p65 and p65 (not shown). There were some noticeable differences between 4 and 6 Wks. sample counterparts, such as the level of expression. However, due to the limitations of DAB based immunohistochemistry as a quantitative tool, significance could not be calculated from these results. It was observed that in general, cytoplasmic localisation was predominant in WT samples. Nuclear localisation is observed in both WT and KO samples, but occurs predominantly in neurons.

3.5.1 Figure 3: 6 Wk. IHC p65 (n=3 for each image)

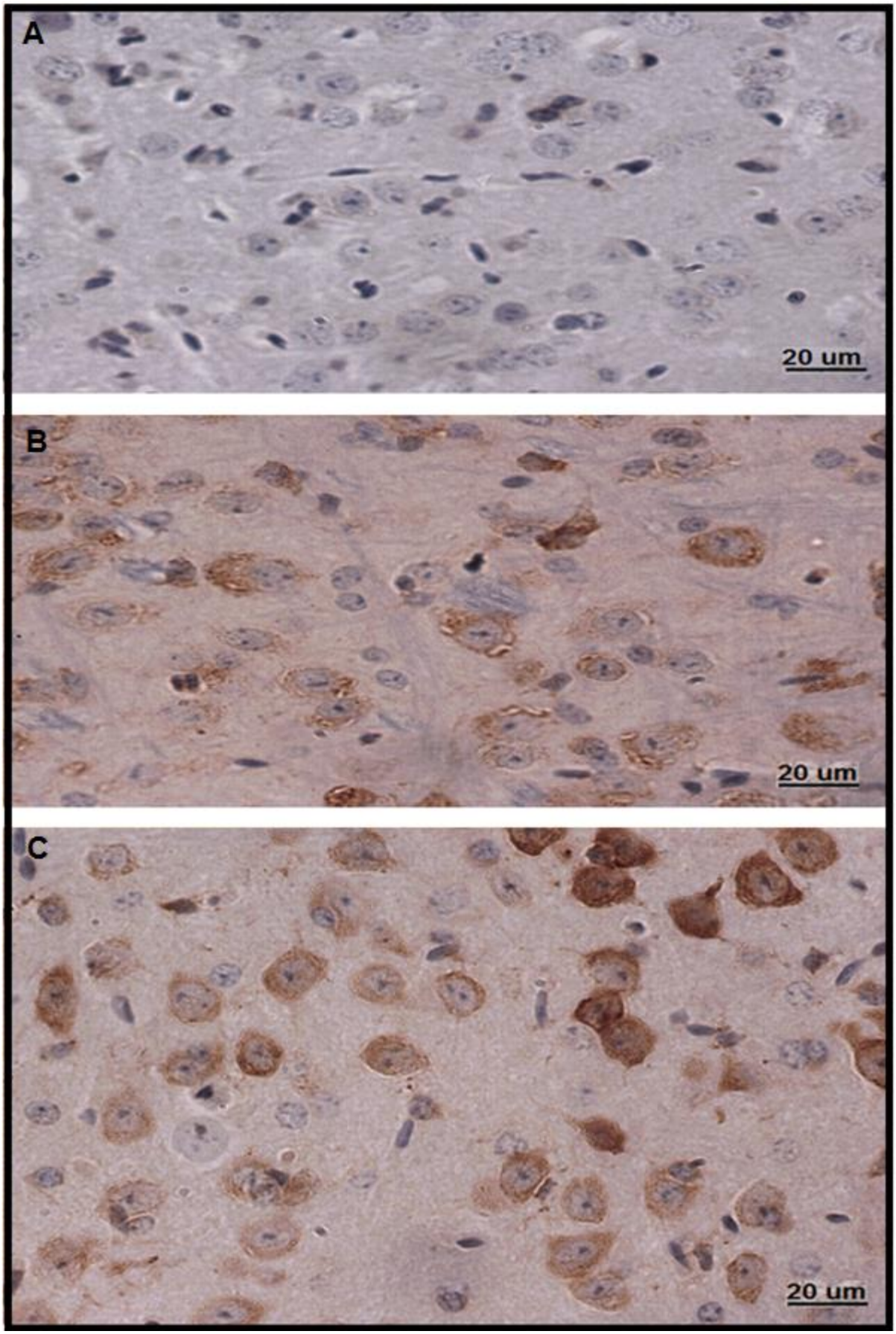

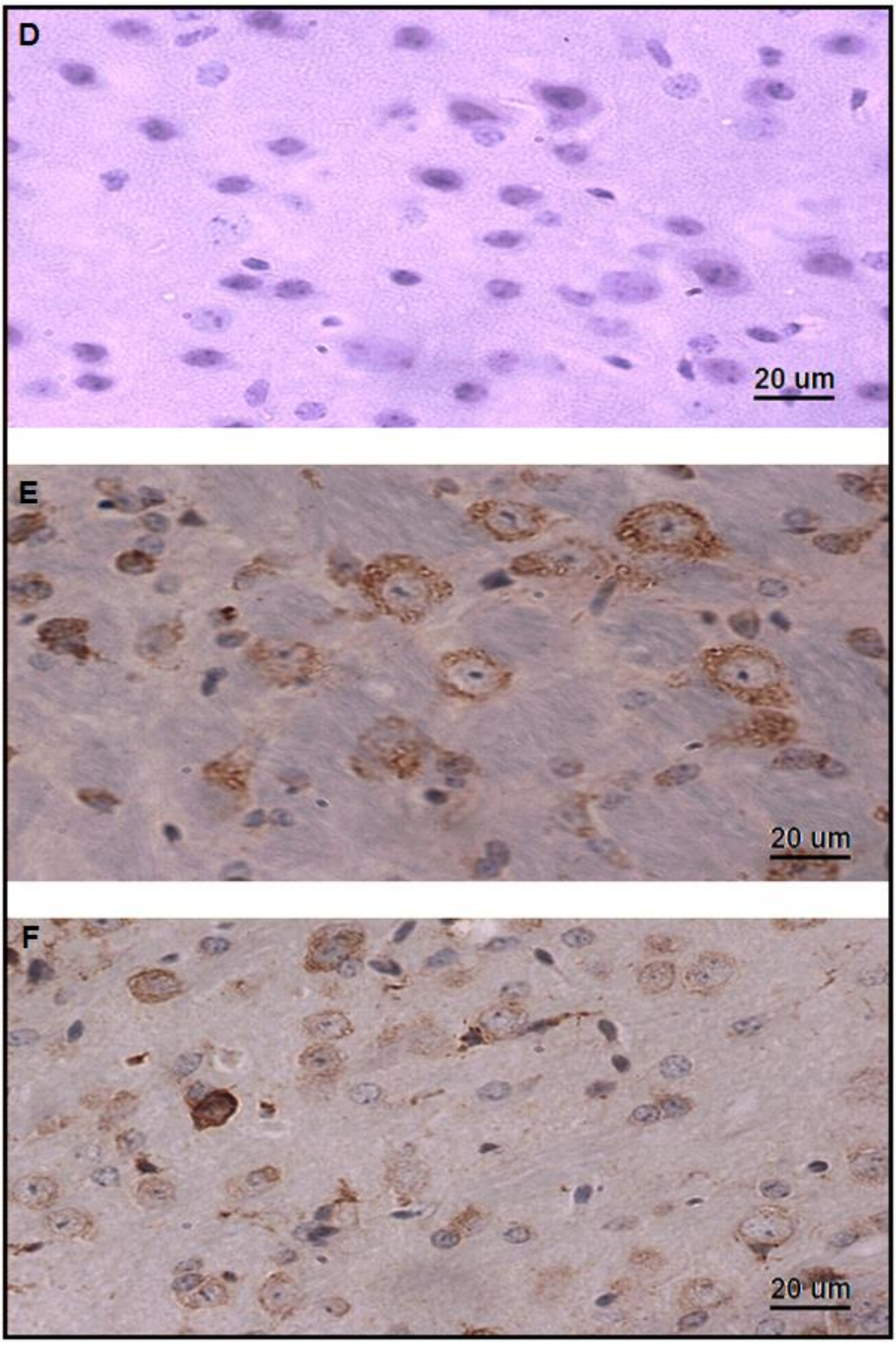
D
20 um
E
20 um
F
20 um

Figure Legend

IHC to visualise the expression and cellular type / localisation of p65 was performed on paraffin embedded samples at 6 weeks. The negative controls were taken from the olfactory bulb, and hippocampus respectively (A, D), (Region of focus for B-C / E-F, forebrain, cortex) the expression and localisation of p65 varies between both sample sets, however appears to be predominantly neuronal. Expression of p65 is the highest in Wild Type (WT) control samples (B, E) when compared to Knock out (KO) samples (C, F). Interestingly, nuclear localisation is more predominant in sample set 1 (B, C), the inverse of this is observed in set 2 (E, F). Images were obtained at x 40 / 0.9 magnification using Axiovision software.

3.5.2 Figure 4: 4 Wk. vs 6Wk. IHC p65 (n=3 for each image

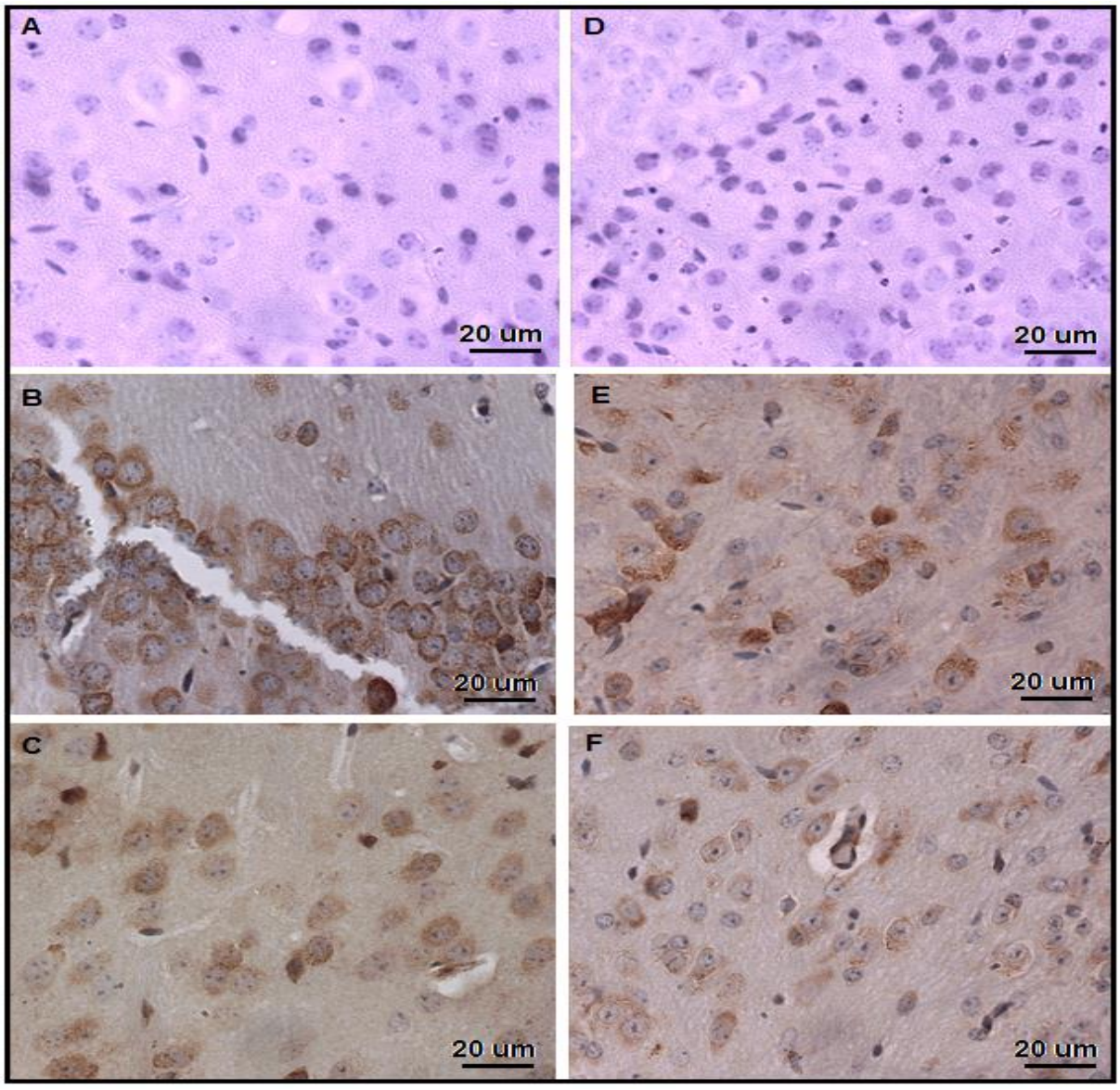

Figure Legend

IHC to visualise the expression and cellular type / localisation of p65 was performed on paraffin embedded samples at 6 Wk. and 4 Wk. (Region of focus; forebrain, cortex). The expression and localisation of p65 was observed to be predominantly cytosolic for both weeks. Expression of p65 is the highest in Wild Type (WT) control samples (B, E) when compared to Knock out (KO) samples (C, F). Images were obtained at x 40 / 0.9 magnification using Axiovision software.

3.6 Immunofluorescent analysis

Immunofluorescence was used as a means of generating positive controls for NF-κB. This technique was used due to the repeated absence of NF-κB in Western analysis, along with the limitations of results procured using DAB immunohistochemistry. This procedure was intended to validate the effectiveness of the primary antibodies used in this study for the subsequent detection of p65. LPS-Stimulated mouse macrophage cells were used, provided by Rockliffe, A. These were post fixed in 4% PFA following dose-dependent LPS exposure. Following IF treatment p65 was observed to be predominantly cytosolic (unlikely) with little nuclear translocation overall.

3.6.1 Figure 5 LPS-Induced mouse macrophage NF-κB positive control (n=1).

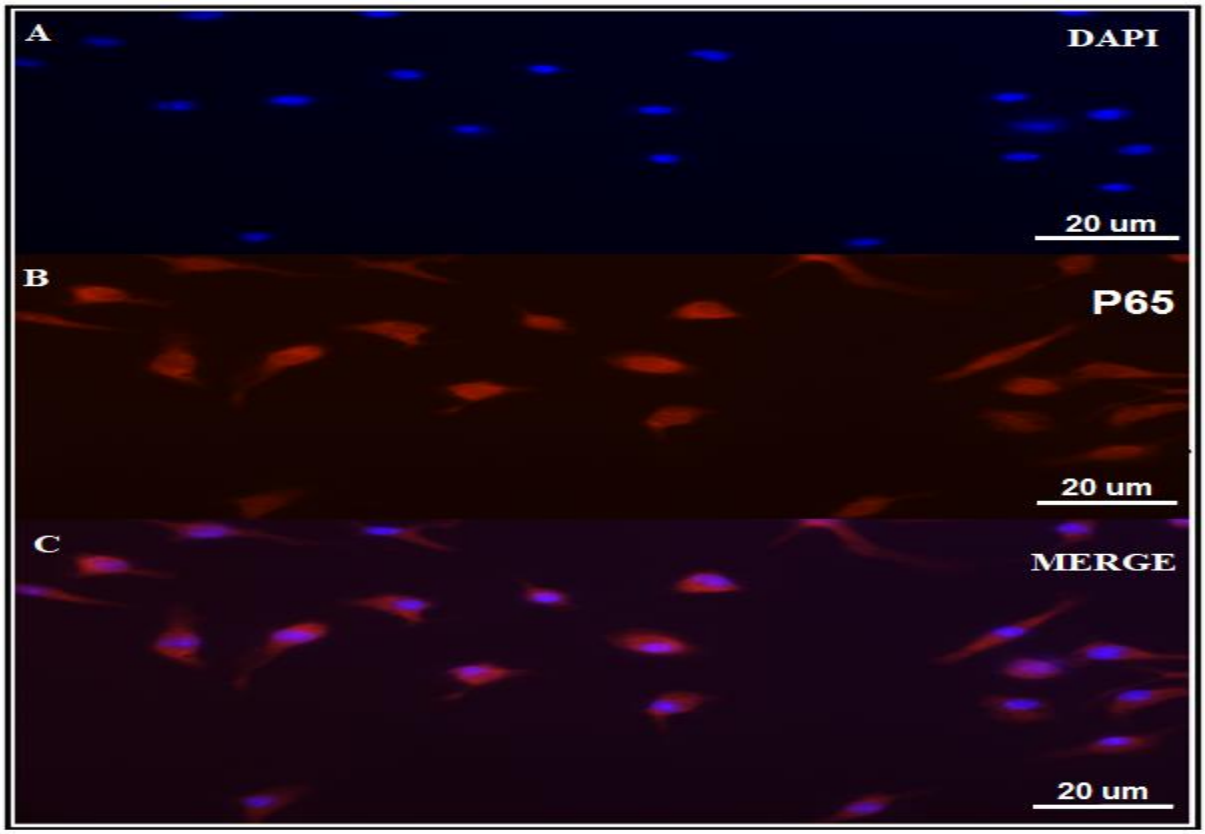

3.6.2 Figure 6 LPS-Induced mouse macrophage NF-κB positive control (n=2).

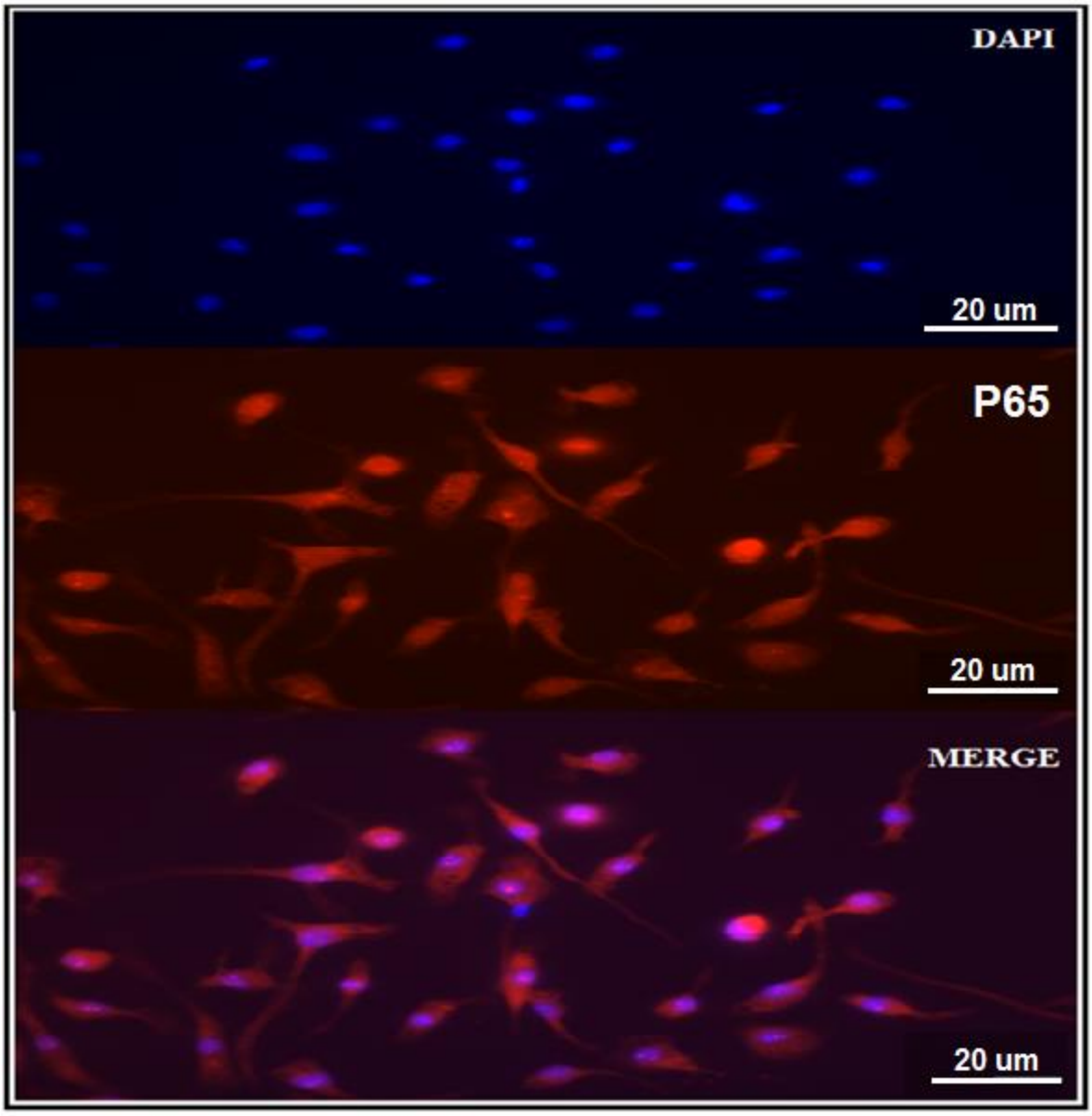

Figure Legend

These figure shows a few, isolated incidences of p65 nuclear translocation. Images were obtained at x 40 / 0.9 magnification using Axiovision software.

P65 results summary

P65 was predominantly undetected. Detection that did occur was found to be neuronal and cytosolic exclusively.

Chapter 4: STAT 1 and STAT 3 Results

4.1 STAT 3 Western analysis

Western Analysis was used to measure the protein expression of STAT-1/3 in samples acquired from 4 and 6 Wks. knock-out (KO) models and compared to Wild Type (WT) controls. WB analysis was able to show quantifiable, significant differences between the KO and WT samples for both STAT-1 and STAT-3. However, further statistical analysis was performed, showing inconclusive results, thus lowering the confidence of the aforementioned results. Selected Western blots for both STAT-1/3 at 4 and 6 Wks. Can be seen below.

4.1.1 Figure STAT-3 and GAPDH Western Blot for STAT-3 at 4 and 6 Wks (n= 6 for all variables).

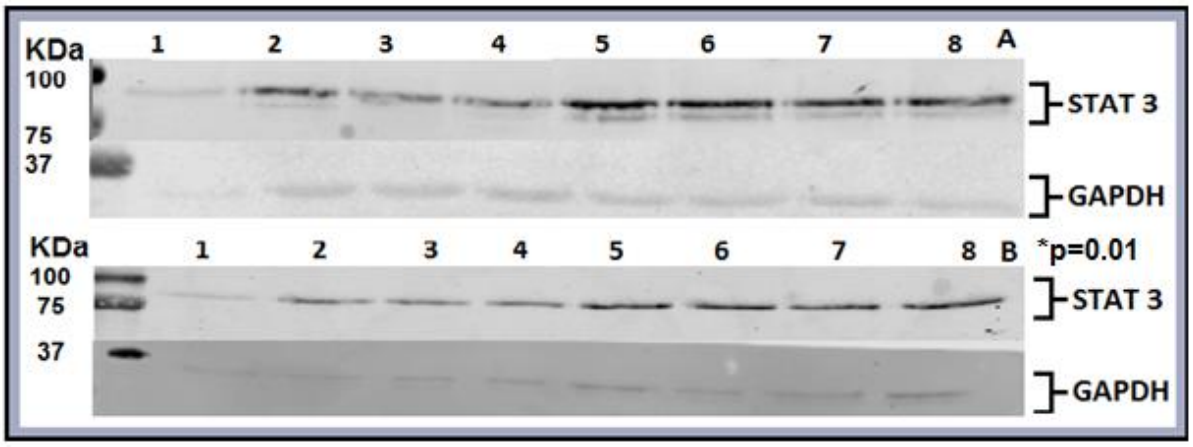

Figure Legend

The analysis of results at 4 (B) weeks showed statistically ($p < 0.05$) relevant differences. Analysis of 6 weeks (A) showed a statistically interesting value of $p=0.07$. One tail analysis ($p=0.035$) suggests a unidirectional relationship in expression. Multiple banding is the result of differential binding to STAT-3 isoforms.

4.1.2 Figure 4 Wk. STAT-3 Fold Difference (%): Mutant vs Control samples (A); Mutant Samples (MS) vs MS mean (B).

Normalised (GAPDH) Mean: 2.998 ***Sample Standard Deviation: 0.227***

4.1.3 Figure STAT 1 and GAPDH Western Blot 3 at 4 and 6 Wks. (n=7 for all variables)

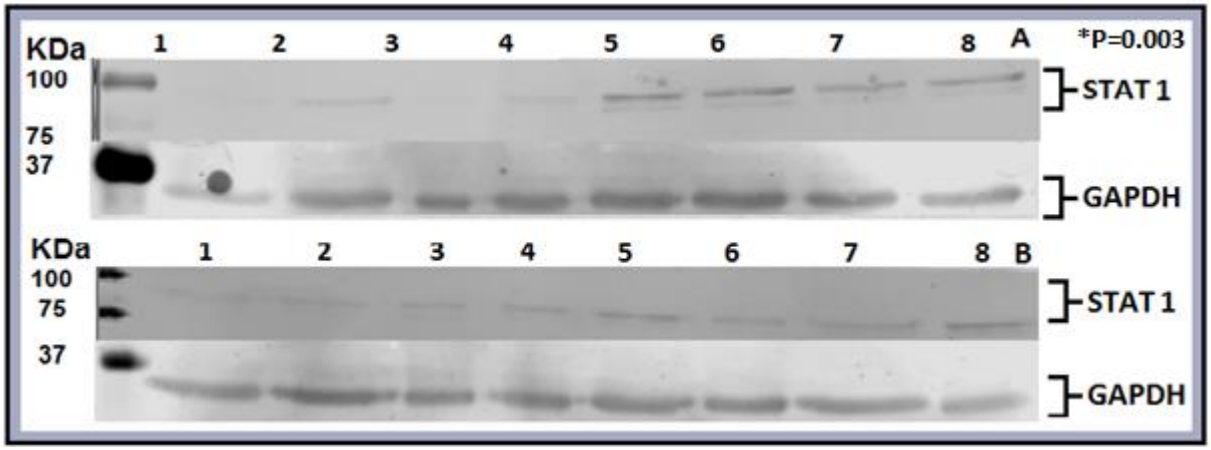

Figure Legend

The analysis of results at 6 (A) weeks showed statistically ($p < 0.05$) relevant differences. Analysis of 4 weeks (A) showed a statistically interesting value of $p=0.06$. One tail analysis ($p=0.033$) suggests a unidirectional relationship in expression. Multiple banding is the result of differential binding to STAT1 isoforms.

4.1.2 Figure 4 Wk. STAT-1 Fold Difference for Mutant samples (A); Mutant Samples (MS) vs MS mean (B).

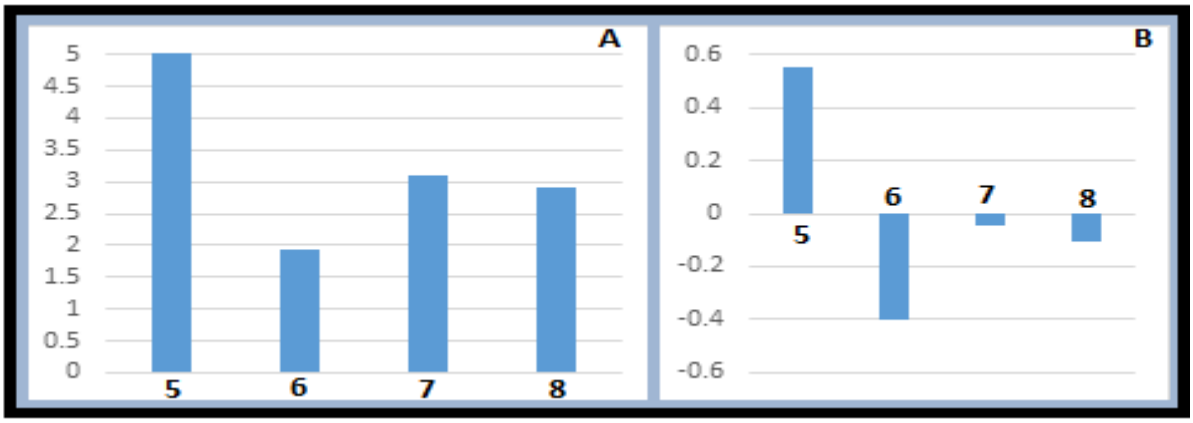

Normalised (GAPDH) Mean: 12.606 ***Sample Standard Deviation: 0.939***

4.2 STAT 1 Immunohistochemistry

STAT 1 expression was measured in WT and KO 4&6 Wks. paraffin embedded perfusion fixed samples, sliced accordingly (5 µm). This was done on a preliminary basis to determine the localisation of STAT 1.There were some noticeable differences between 4 and 6 Wks. sample counterparts, such as the level of expression.

However, due to the limitations of DAB based immunohistochemistry as a quantitative tool, significance could not be calculated from these results. It was observed that in general, STAT 1 localisation was predominantly glial based. Furthermore, the morphological differences between cells expressing STAT 1 can be seen in control vs KO, such as an increased cell volume and 'darker' expression of DAB.

4.2.1 Figure 6 Wk. STAT 1 IHC (n= 1 for each).

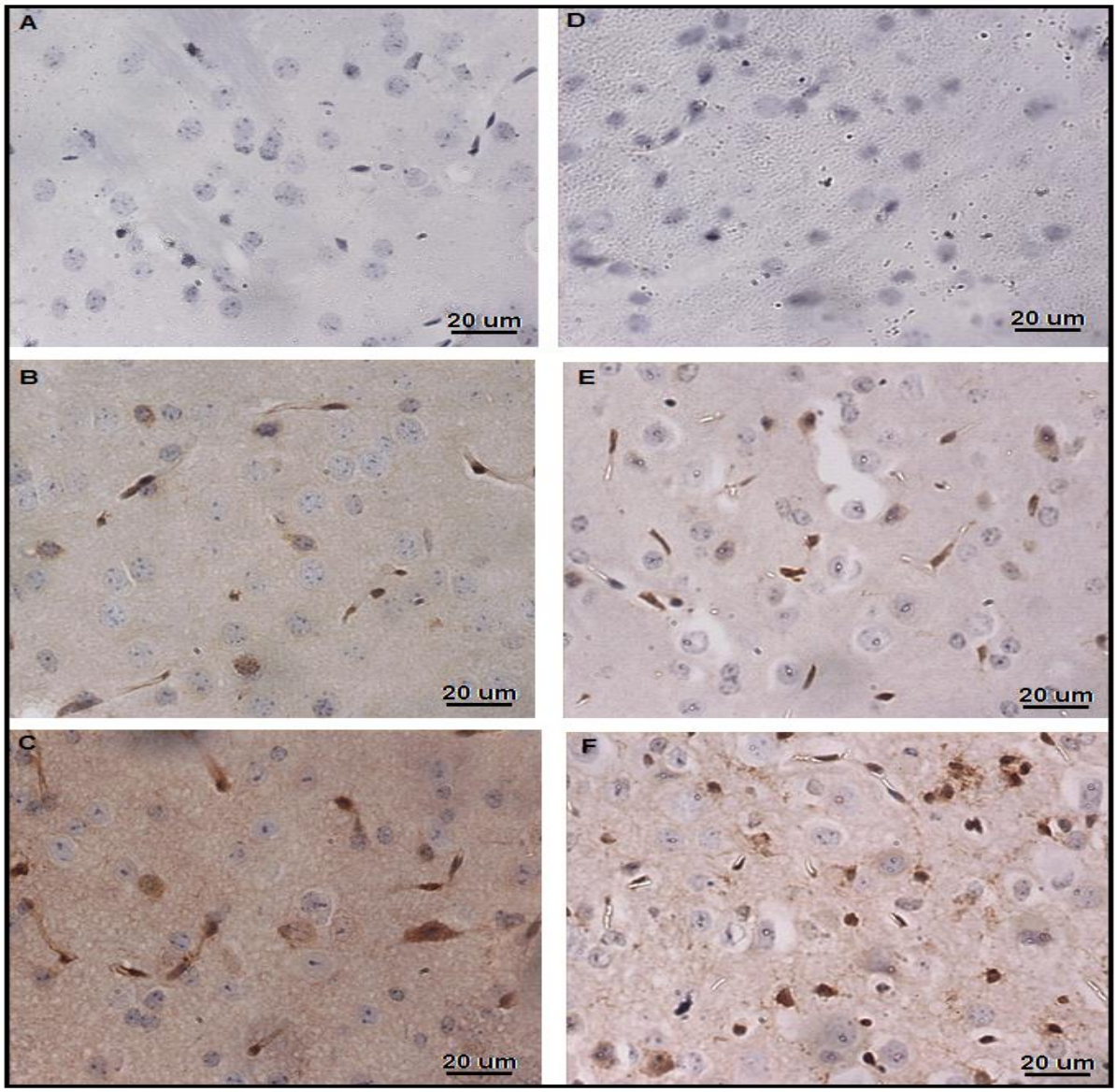

Figure Legend

IHC to visualise the expression and cellular type / localisation of STAT 1 was performed on paraffin embedded samples at 6 Wk. and 4 Wk. (Region of focus; forebrain, cortex). There is an increased cell count (visual) at 6 Wks. Vs 4. Alongside this, physiological differences indicate reactivity. Images were captured at x40 / 0.9 magnification using Axiovision software.

4.2.1 STAT 1 Immunofluorescent analysis

Immunofluorescent analysis for STAT 1 was utilised to allow a more thorough observation of its cellular dynamics. This was used due to the limitations of DAB immunohistochemistry previously outlined. The key findings of this analysis are as follows: It was observed that STAT 1 localisation was predominantly glial. Furthermore, WT STAT 1 expression was perceived to be exclusively cytosolic. In respect to KO samples, findings were considerably varied. In general, STAT 1 Nuclear localisation was seen, with affected regions illustrated below. Distinguishing between STAT 1 (Red) and background diffraction was performed on a qualitative basis. All images were captured at x40 / 0.9 magnification using Axiovision software.

4.2.2 4 Week STAT 1 Control (WT).

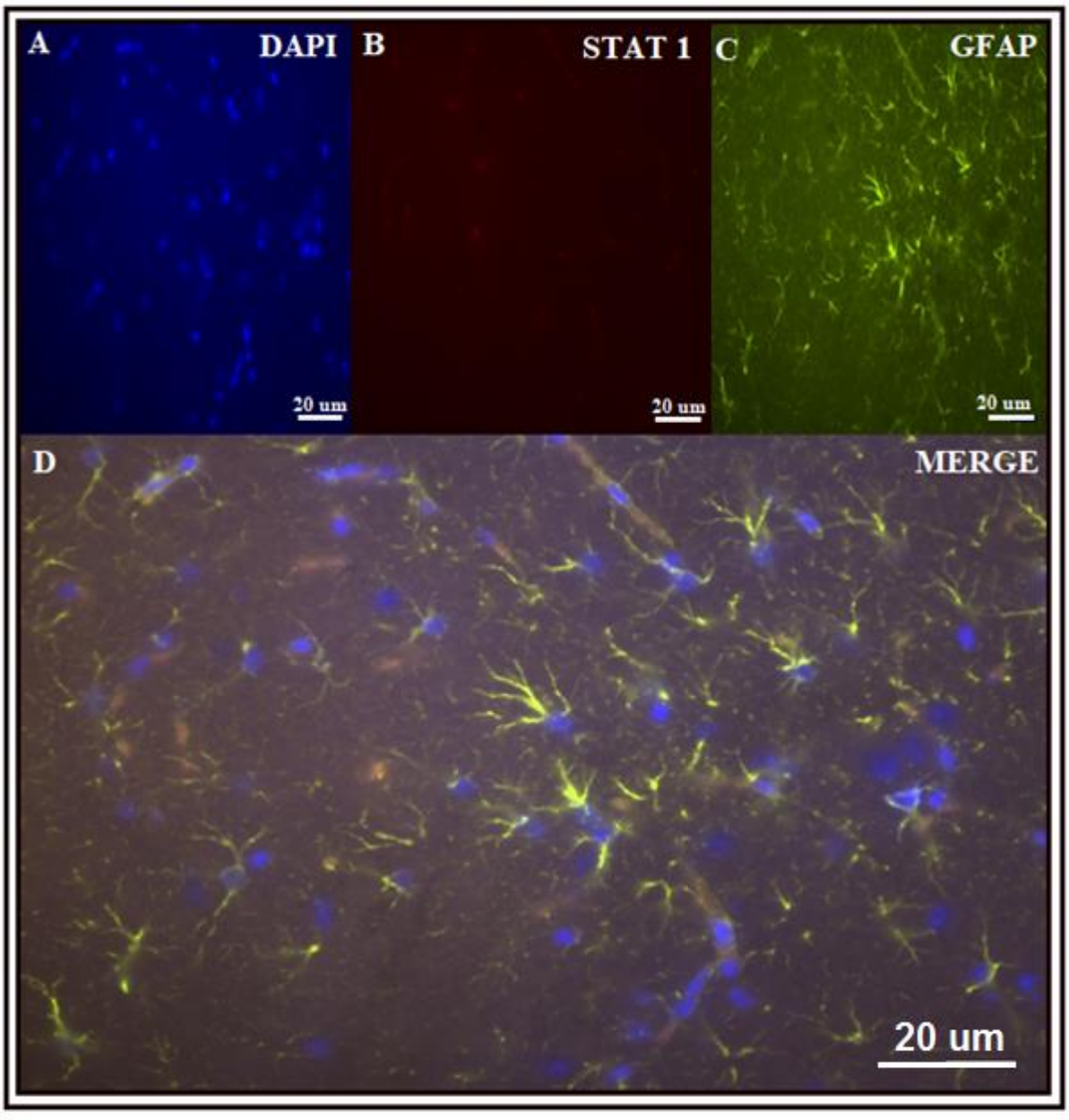

Figure Legend

STAT 1 (B: Red) was seen to have a low expression level (Region of focus; forebrain, cortex). Furthermore, no incidences of nuclear (A: Blue) translocation were observed. Reactive astrogliosis, measured using GFAP (C: Yellow) was limited/not observed (Total Area: 3.17%).

4.2.3 4 Week STAT 1 psmc1 mutant (KO).

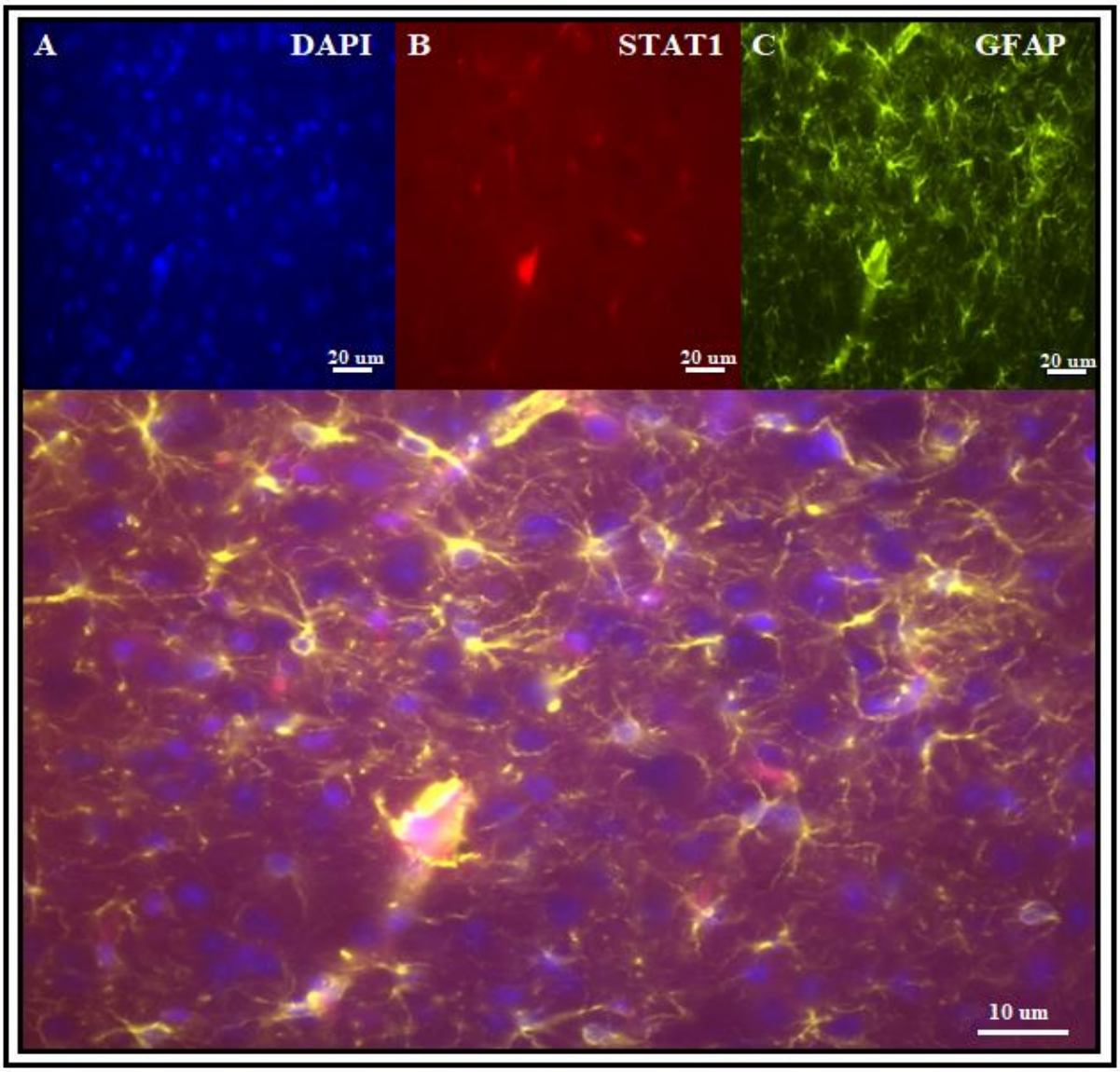

Figure Legend

STAT 1 (B: Red) was seen to have a higher expression level (Region of focus; forebrain, cortex). Furthermore, there were a few, no significant incidences of nuclear (A: Blue) translocation observed. Reactive astrogliosis, measured using GFAP (C: Yellow, Total Area: 11.5%) was markedly increased, often corresponding to regions exhibiting STAT 1 nuclear translocation.

4.2.4 6 Week STAT 1 Control (WT)

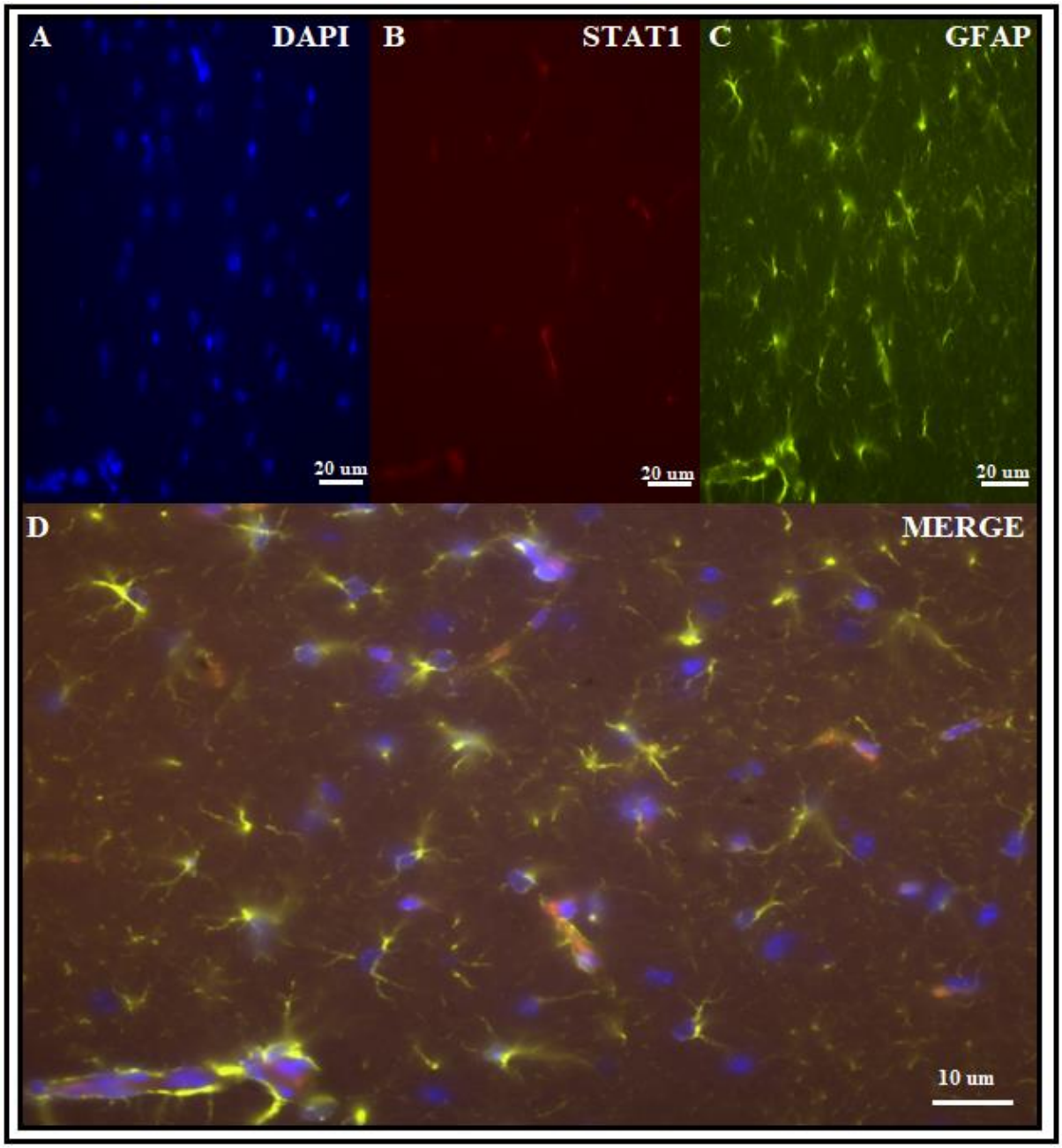

Figure Legend

STAT 1 (Red) was seen to have a low expression level (Region of focus; forebrain, cortex). Furthermore, no incidences of nuclear (Blue) translocation were observed. Reactive astrogliosis, measured using GFAP (Yellow) was limited/not observed. (Total Area: 4.91%)

4.2.5 6 Week STAT 1 psmc1 mutant (KO)

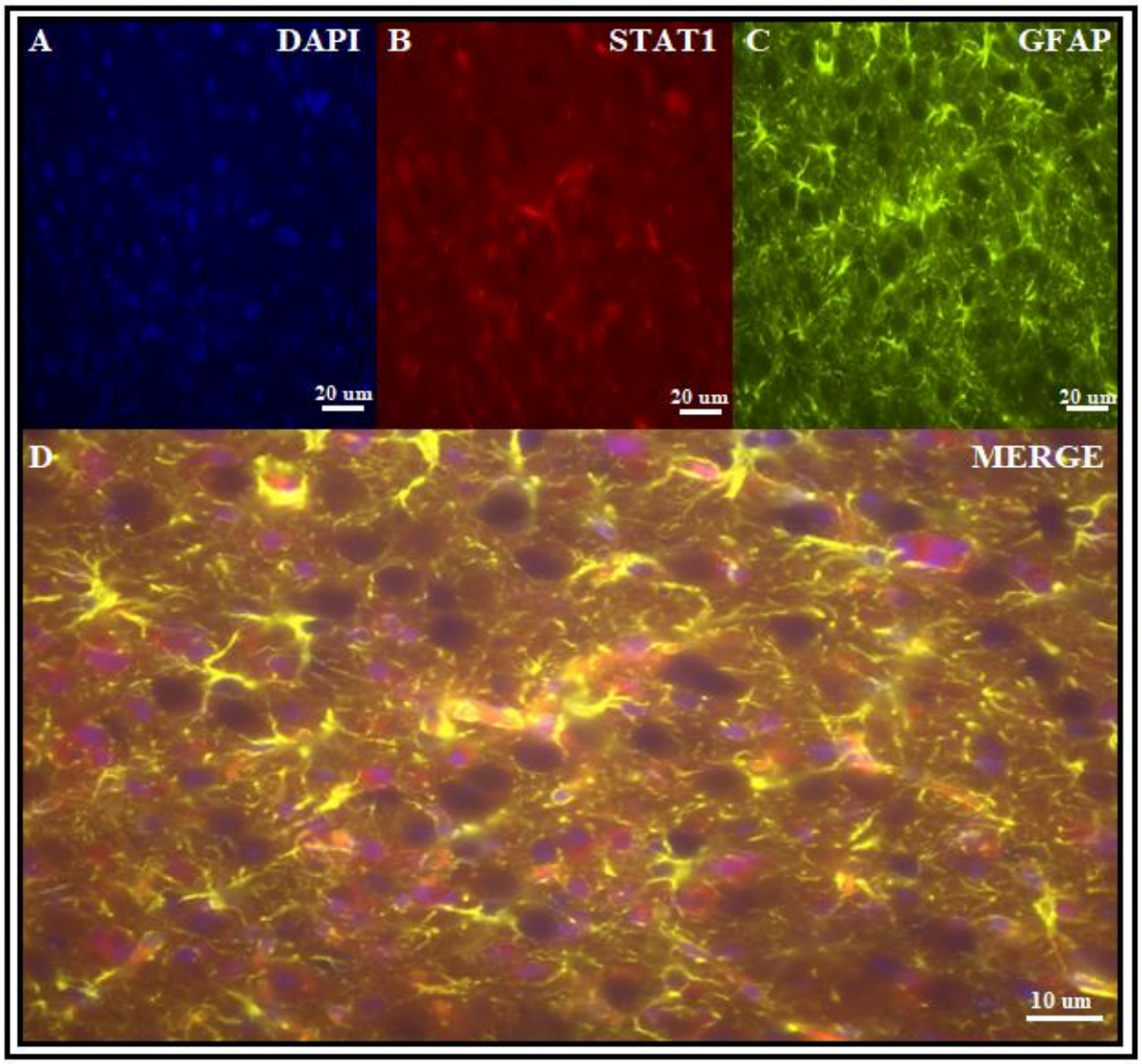

Figure Legend

STAT 1 (Red) was seen to be ubiquitously expressed in all non-neuronal cells (Region of focus; forebrain, cortex). Furthermore, numerous incidences of nuclear (Blue) translocation were observed. Reactive astrogliosis, measured using GFAP (Yellow) was markedly increased (Total Area: 11.19%).

4.3 STAT 1 and 3 results summary

STAT 1 and 3 appear to have an inversed relation of expression. Thus STAT 1 is expressed to a greater extent at 4 Wks. Followed by a decline in expression.

Chapter 4: Discussion

4.1 Measuring Neuroinflammation

Typical hallmarks of neuroinflammation were observed, further illustrated in Chapter 3. Furthermore, other experimental data indicates a distinct localisation and proliferation of glial cells. Specifically, astrocytic reactivity was observed in both immunohistochemical and further immunofluorescent analysis. This was measured using the expression of Glial Fibrillary acidic Protein (GFAP). This was chosen due to it ubiquitous role in astrocytic processes. Microglial analysis utilised IBA1 tagging. It was observed that microglia underwent physiological developments when comparing results from 6 and 4 Wks. Along with the observed changes, microglial proliferation also occurred. GFAP specific Immunofluorescent analysis was able to show quantifiable differences between WT and KO at both 4 (3.17-11.5 %) and 6 Wks. (4.91-11.19 %). This indicates that the disruption of the UPP via progressive dysfunction of the 26S Proteasome is correlative with increased astrocytic reactivity and other hallmarks of neuroinflammation. These findings corroborate previous discussions have shown markers of degenerative neuroinflammation. Preliminary astrocyte (GFAP) analysis showed an increased density and connectivity of astrocytes in KO models. The increased staining of GFAP indicates an increased expression / expansion of astrocytic processes. These findings, along with the localisation of the astrocytes (predominantly in regions that have shown stereotypical neurodegeneration in previous studies) would suggest a difference in the KO model is responsible for the increased reactive astrogliosis observed versus WT.

4.2 STAT and NF-κB: the relationship they have with UPP-dysfunction induced inflammation.

In order to determine by which pathways UPP dysfunction induces neuroinflammation, the NF-κB and STAT transcription regulation families were investigated. Defining the precise roles of p65 and STAT1/3 in the neuroinflammation investigated as a result of neuron-specific 26S proteasome depleted (knock-out) mice [Psmc1] proved to be challenging.

4.3 P65 detection and localisation.

The repeated absence of banding appropriate for p65 during western analysis would indicate a lack of involvement in neuroinflammation in the WT and KO model samples. This is highly suspicious, as the NF-κB canonical pathway is a fundamental inflammatory regulator. However, with histological analysis, neuronal p65 nuclear localisation was occasionally observed at various weeks (Fig. 3, 4), painting a contrasting picture.

This observed localisation may account for the favourable p65 expression seen in nuclear extraction samples at 5 weeks (Fig.1). Previously, p65 has been shown to be constitutively expressed in neuronal cytoplasm for normal cellular function (56). However, in all histological preparations, neuronal cytoplasmic p65 is most concentrated in WT samples (Fig.3 E, Fig.4 B, and E). In corresponding KO samples, (Fig3 F, Fig.4 C, F) cytoplasmic p65 localisation was decreased. Interestingly, this coincides with increased, albeit sporadic nuclear localisation. This may suggest neuron specific p65 activation, which has been observed both constitutively and in regulatory capacity in numerous previous studies. Furthermore, when samples are compared (4 Wks. vs 6 Wks.) p65 concentration appear to decrease. This unexpected decrease requires further investigation. Unfortunately, this was not achievable due to a lack of sufficient translocation in a p65 positive control (see 3.3 Figures 5 and 6). This could suggest that the antibodies chosen to conduct this study were ineffective at detection and subsequent binding. However, it is also likely that the inconclusive nature of the results obtained were due to technical issues and shortcomings as well. The neuron-specific localisation of p65 was unexpected. The observed localisation may be a matter of coincidence due to constitutive p65 localisation as previously discussed. Conversely, due to the dynamic regulatory capabilities of p65, the observed localisation may impact neuroinflammation.

4.3.1 Constitutive neuron p65 activation and the progression of inflammation.

Through transcriptional regulation, p65 regulates the production and secretion of cytokines, such as TNF-α. Unregulated protein aggregation is a known inducer of inflammation. Thus, progressive, age related neuronal p65 activation could contribute to neuroinflammation by the increased production of inflammatory mediators, as well their respective receptors, such as Toll-like receptors. This would lead to the activation of numerous inflammatory pathways (JAK/STAT). In regards to specific causes of neuroinflammation seen in the KO model used for this research, intra-neuron polyubiquinated inclusions may signal and activate the constitutive cytoplasmic ‘cache’ of p65 to localise to the nucleus and alter the neuron specific transcriptome. However, in light of inconsistent nuclear translocation, it could be said another mechanism related to NF-kB, is responsible (see Iκβα). Due to the difficulties in NF-κB’s detection, along with consistent data proving to be so elusive, it cannot be said with any certainty the role NF-kB’s plays in orchestrating UPP-mediated neuroinflammation.

4.3.2 Measuring Iκβα degradation.

Iκβα was measured as means to follow p65 activation. Due to the prerequisite need for Iκβα degradation to enable p65 activation, protein expression was measured to see if decreased concentrations might indicate p65 activation indirectly. Surprisingly, Iκβα expression did not differ between WT and KO samples at 4 or 6 Wks. (Fig.2 A, B). However, it appears to have a decreased expression at 4 relative to 6 Wks. This might account for the increased p65 staining in 4 Wk. histological samples (Fig.4 B, C) by virtue of decreased Iκβα concentration. This case could be argued by the reduced age of the samples, which would have a comparatively reduced decline in UPS function. This would require further validation, such as an observable increase in Iκβα in 6 Wk. KO samples, which did not occur. Another means by which p65 indirectly affects inflammation is via the poly-ubiquitination of Iκβα.

4.3.3 Repressed intraneuronal Iκβα degradation could contribute to inflammation.

The accumulation of ubiquitylated Iκβα, due to its association with neuron-specific constituently expressed p65 may aid in inducing the rampant neuroinflammation seen in this model. If this were the case, inflammation would be achieved by the activation of intraneuronal transcription regulators, such as the STAT family. This would be measured in 26S depleted ubiquitin rich neuron inclusions. Subsequently, if the outlined mechanism is the means of action, inflammatory transcriptional regulation would result in the production and secretion of inflammation mediators- such as cytokines. Furthermore, the resulting cytokine storm and reactive gliosis could be seen to be initiated indirectly by p65 via Ub-Iκβα. This would need the coordinated comparison of transcriptomic analysis (potentially using RNAseq or qPCR) to measure transcriptomic differences along with protein concentration determination. This is required to determine if Ub- Iκβα makes up a significant percentage of the neuronal ubiquitin inclusions found in this model. Furthermore, if Ub- Iκβα does indeed make up a large portion of the neuronal inclusion, how does that directly affect transcriptional regulation? Exploring the above pathways may yield a means of validating NF-κB ’s role in inflammation seen in the mutant model.

4.4 STAT 1 detection and localisation.

Western Analysis from 4 and 6 Wks. knock-out (KO) models vs Wild Type (WT) controls showed quantifiable, statistically significant differences between the KO and WT samples for STAT 1. However, further statistical analysis (see appendices, 12) was performed, showing inconclusive results, thus lowering the confidence of the aforementioned results. Selected Western blots analysis at 6 (A) weeks showed statistically ($p< 0.05$) validated increased in STAT 1 expression in mutant samples. Analysis of 4 weeks (A) showed a statistically interesting value of $p=0.06$. One tail analysis ($p=0.033$) would suggest a unidirectional relationship in expression. However, this cannot be taken to be significant due to the variable confidence in the experimental data procured in this study. Further experimentation would be required to establish the significance of this cursory observation. The mode of action that results in the differences seen between 4- and 6-week expressions were not elucidated in this study. This difference could be due to an insufficient time frame having lapsed post the initiation of 26S proteasome depletion in 4 Wk. samples to significantly alter STAT 1 expression. To determine the extent of activation and localisation of STAT 1, histological analysis was performed. Initial preliminary DAB immunodetection to determine the cell-specific localisation of STAT 1 showed a predominant glial preference. Interestingly, this contrasts with the aforementioned neuronal localisation of p65. In addition, there were some noticeable differences between 4 and 6 Wks. sample counterparts, such as the level of expression, determined by visually comparing the relative darkening of tagged regions. However, due to the limitations of DAB based immunohistochemistry, this could not be attributable to differences in protein expression. Interestingly, the morphological differences between cells expressing STAT 1 can be seen in control vs KO, such as an increased cell volume. This in conjunction with preliminary neuroinflammatory analysis (IHC of IBA-1 and GFAP) show a visual similarity. This hints at STAT-1's involvement in driving the prerequisite phenotypical remodelling of glial architecture seen in CNS inflammation. To provide clarity of cell type and further precision of sub-cellular location, Immunofluorescence was performed to observe STAT 1 in relation to astrocytes (GFAP). Overall, STAT 1 expression was minimally increased in 4 Wk. KO when compared to 6 Wk. samples. This was expected due to the results of western analysis indicating STAT 1's insignificance at 4 Wks. Conversely, the marked increase in expression and glial-specific nuclear translocation at 6 Wks. was in accordance with the results.

4.4.1 STAT 3 expression in relation to STAT 1.

STAT 3 was shown to follow an inversed pattern of expression in relation to STAT 1. However, it must be considered that a similar variability and inconclusiveness was seen in STAT 3 data as well. Statistical analysis (not shown) shows a significant correlation between the age related differences in expression between STAT 1 and 3. Simply, this suggests a time dependent negative correlation between the STAT proteins. However this cannot be taken at face value, due to the variance in observation conditions between data sets. Histochemical analysis was not performed, this is because previous observations yielded conclusive evidence of the antibodies effectiveness, and thus Immunofluorescence was performed straight away. However, despite previous examples of successful preparation by colleagues, STAT 3 Immunofluorescent analysis yielded no results. In order to determine the precise relationship between STAT 1and 3, further experimentation is needed. It is known that STAT1 and 3 heterodimerise in order to bind to GAS sites. This joining alters the set of inflammatory genes the complex is able to regulate. Current observation would suggest this dimerization does not take place (due to inverse protein expression), however this cannot be ruled out. Time varied Co-precipitation and immunofluorescent analysis would allow a more thorough investigation of their dependence on one another.

4.5 Generation of cre-lox psmc1 (26S Proteasome) delayed knockout phenotype- Bedford, L et al, 2008.

Generation of the LBD mouse model used in this study was undertaken previously by Bedford, L. This was achieved using cre-lox recombination technology along with selective out breeding to produce site specific 26S proteasome functional decline. Initially, floxed Psmc1 mice were generated using homologous recombination. Specifically, a loxP-flanked neomycin-thymidine kinase selection cassette and a loxP site were inserted into introns 1 and 3, respectively, of the Psmc1 gene (Gene ID 19179) in mouse 129/Sv embryonic stem (ES) cells. The selection cassette was subsequently excised, achieved by transient expression of Cre recombinase in vitro. Forebrain-specific ablation of Psmc1 (and thus 26S proteasome function) was achieved by crossing Psmc1 fl/fl mice with CaMKII-Cre mice (Lindeberg et al., 2002). CaMKIIα-Cre transgenic mice have the mouse calcium/calmodulin-dependent protein kinase II alpha promoter (CaMKIIα) directing expression of Cre recombinase. When the CaMKII-Cre mice is crossed with a strain containing loxp site flanked sequence of interest, Cre-mediated recombination occurs in the pyramidal cell layer.

When this strain was crossed with the previously generated floxed Psmc1 mice, the resulting genotype of the offspring was: Psmc1 fl/wt;CaMKII-Wt and Psmc1 fl/wt;CaMKII-Cre mice. Subsequent to this**,** female Psmc1 fl/wt;CaMKII-Cre mice were mated with homozygous floxed Psmc1 males. This produced littermates in which Psmc1 was selectively inactivated in calcium calmodulin-dependent protein kinase II-expressing cells (Psmc1 fl/fl; CaMKII-Cre) and appropriate control mice (Psmc1 fl/fl;CaMKII-Wt or Psmc1 fl/wt; CaMKII-Wt). Previous histological analysis of brains from both control and Psmc1 fl/fl;CaMKIIα-Cre mice indicate significant, progressive atrophy of the forebrain. This was observed due to a marked reduction in the cortical thickness, alongside an expansion of the ventricular cavities. At 2 weeks of age, there were no degenerative changes evident in the Psmc1 fl/fl;CaMKIIα-Cre forebrain. However, at 4 weeks numerous pyknotic nuclei became apparent, which become more abundant by 6-weeks. This accumulation precedes the extensive neuronal loss seen at 8 weeks. The development of pyknotic nuclei indicate an apoptotic mechanism of neurodegeneration. Interestingly, this was confirmed by the upregulation of cleaved caspase-9 (A well-established marker of apoptosis). Furthermore, decreased Bcl-2 expression was observed in the model. Immunohistochemical staining with GFAP demonstrated extensive astrocytic gliosis accompanied with neuronal loss in the cortex of mutant samples. Neurodegeneration was evident in other CaMKIIα-expressing regions of the Psmc1 fl/fl;CaMKIIα-Cre brain, including the hippocampus, striatum, and amygdala .

4.6 Future developments and potential of current research.

This study could be the basis for future research in numerous ways. Firstly, NF-κB activation was far too obscure and limited to formulate a coherent hypothesis for its mechanism of action. This could be tackled firstly by performing the appropriate controls for determining the effectiveness of the antibodies used in its detection. Once a reliable method for detection has been created, the potential for tracking p65 changes in this model will undoubtedly increase. STAT 3 localisation also requires further investigation than it could be afforded in this study due to time constraints / technical difficulties. Once this fundamental knowledge is established, the limitations of this study will be significantly reduced. This could be followed by a plethora of avenues through which a greater understanding of neuroinflammation will be achieved. The potential interdependent relationship between STAT 1 and 3 in this model would be a strong starting point. The tentative notion that the STAT 1 and 3 expression / activation could be examined by Co-IP as previously mentioned. In conjunction to this, an interdisciplinary approach would yield a greater range of results from which a more concrete hypothesis may be formulated. In order to achieve this, transcriptomic analysis of both glial and neuron cells would be performed *in vitro* using known inducers, such as diallyl disulphide in the case of STAT 1. From this, the strongest candidate pathways activated in cell specific pathways will be observed. Due to the interdependent nature of CNS inflammation, mechanisms of Neuron-glial interactions *in vivo* would be investigated using the transcriptomic analysis outlined as its basis. This would be done in a comparative manner, exploring the key differences between toxic neuronal inclusion and healthy neuronal interactions with glial cells. This exploratory process can be simplified as follows: 1. Remove limitations of current study by fully determining the expression and localisation of STAT 3 and p65. 2. Determine the precise nature of the relationship between STAT 1 and 3, which will either corroborate the results already obtain or provide suitable alternatives. 3. Determine the protein specific composition of intraneuronal ubiquitin rich inclusions seen in the model. This will elaborate upon the aforementioned notion that Ubiquitin-tagged IκBα. 4. Perform Cell-specific transcriptomic analysis (in vitro) to compare with Western / IHC/IF. 5. Establish the mechanism of action and importance of cell-specific responses to UPP induced neuronal inclusions. 6. Determine the interdependence of the cell-specific response to UPP inclusions as the basis for the observed increase in the neuroinflammatory hallmarks (predominantly reactive astrogliosis) in the model.

Chapter 5: Conclusion

Irrespective of the apparently absent role of p65 within the KO model, the synergistic, current knowledge and understanding of the interdependent nature of the neuroinflammatory response would suggest its activation in some capacity. Thus, the results of this study pertaining to NF-κB are incredibly suspect. This lack of confidence is the result of two main factors. Firstly, the repeated absence of appropriate Western analysis banding. The lack of sufficient nuclear localisation, which was used as the benchmark for activation was apparent to in positive controls conducted to evaluate the usefulness of the p65 antibodies used. STAT-1 and STAT-3 multi-technique analysis was able to show time dependent differences in expression and localisation. However, these differences were not reproducible / statistically significant. As it stands, a proposed model of UPP related neuroinflammation has been outlined. This has been formulated in light of the limited results, and would require a more rigorous and interdisciplinary analysis for further validation.

The accumulation of ubiquitin rich neuronal inclusion and increased reactive astrogliosis is either:

- Independent of NF-κB or aided indirectly via the increased accumulation of faulty proteins, such as Iκβα-Ub.

Subsequently, neuron-inclusion mediated cytokine production leads to the increased synthesis and activation of STAT-1 in glial cells at 4 weeks, 1.5 weeks post 26S Proteasome decline. The activation of STAT-1 results in homo/heterodimerisation, and subsequent nuclear translocation.

Dimer specific binding leads to the increased expression of a distinct subset of cytokines and intracellular inflammatory regulators. This leads to a total increase in STAT 3 expression. The localisation and role this plays in neuroinflammation is unknown. However, this could be related to the stunted increase in astrocytic reactivity seen at 6 weeks if STAT 3 expression is an anti-inflammatory counter measure. An illustrated outline of this hypothetical model can be seen below.

5.1 Proposed model of 26S functional decline related neuroinflammation

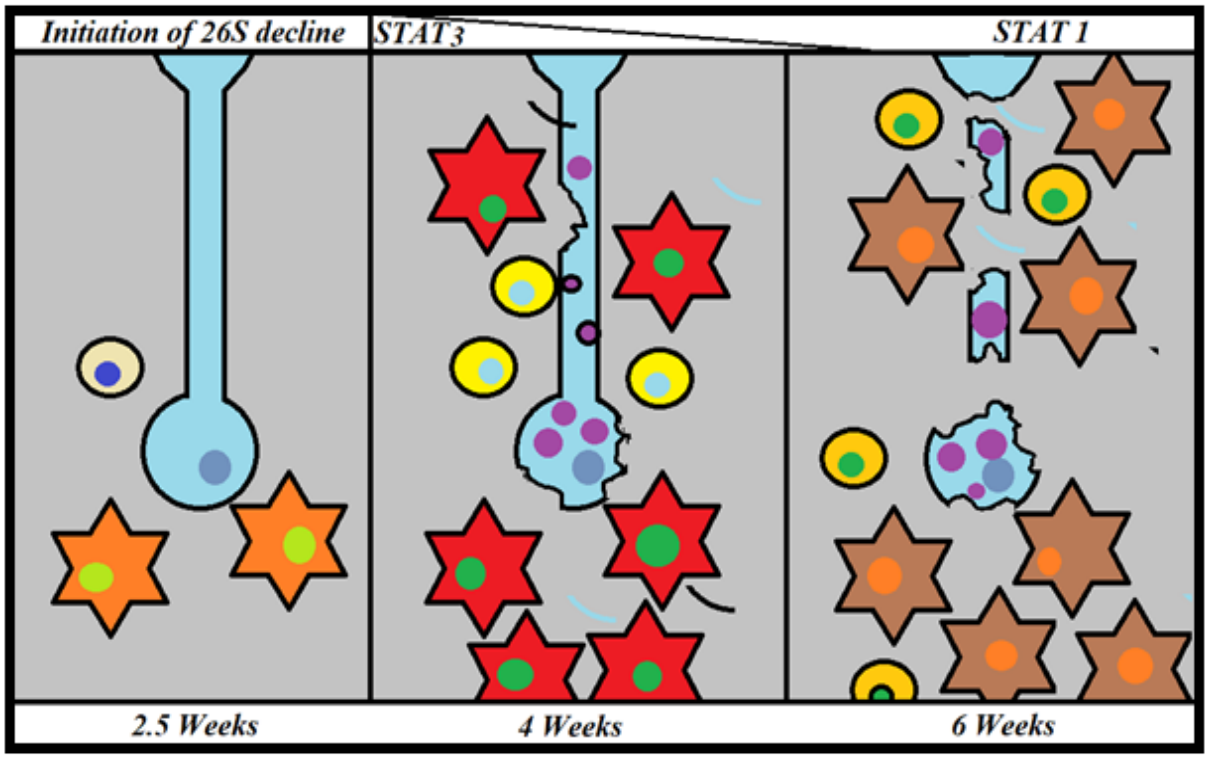

Figure Legend

26S depletion, commencing from 2.5 weeks leads to the development of ubiquitin rich inclusions. These inclusions lead to the localisation and proliferation of microglial cells. These glial cells exhibit increased expression and activation of STAT 3 at 4 weeks. Following the activation of STAT-1, anti-inflammatory cytokine release results in the down regulation of STAT 3 in favour of STAT-1. This change in expression may be related to the relatively decreased astrocytic proliferation than expected that was observed. Thus, STAT-3 is proinflammatory, whereas STAT 1 is anti-inflammatory.

Citations

1. Frakes, A.E., L. Ferraiuolo, A.M. Haidet-phillips, L. Schmelzer, L. Braun, C.J. Miranda, K.J. Ladner, A.K. Bevan, K.D. Foust, J.P. Godbout, P.G. Popovich, D.C. Guttridge, and B.K. Kaspar. 2014. Article Microglia Induce Motor Neuron Death via the Classical NF- k B Pathway in Amyotrophic Lateral Sclerosis. : 1009–1023.

2. Streit, W.J., R.E. Mrak, and W.S.T. Griffin. 2004. Microglia and neuroinflammation : a pathological perspective. 4: 1–4.

3. Haim, X.L. Ben, X.K. Ceyze, X.M.A.C. Sauvage, F. Aubry, M. Guillermier, M. Ruiz, F. Petit, D. Houitte, E. Faivre, M. Vandesquille, R. Aron-badin, M. Dhenain, N. De, P. Hantraye, E. Brouillet, G. Bonvento, and X.C. Escartin. 2015. The JAK / STAT3 Pathway Is a Common Inducer of Astrocyte Reactivity in Alzheimer ' s and Huntington ' s Diseases. 35: 2817–2829.

4. Wenfei Kang Jean M. Hébert. 2012. Signaling Pathways in Reactive Astrocytes, a Genetic Perspective. Dep. Neurosci. Genet. Kennedy Build. Albert Einstein Coll. Med. 1410 Pelham Parkw. South, Bronx, NY 10461, USA. 43: 147–154.

5. Chen, F., V. Castranova, X. Shi, and L.M. Demers. 1999. New Insights into the Role of Nuclear Factor- kB , a Ubiquitous Transcription Factor in the Initiation of Diseases. 17: 7–17.

6. Bedford, L., D. Hay, A. Devoy, S. Paine, D.G. Powe, R. Seth, T. Gray, I. Topham, K. Fone, N. Rezvani, M. Mee, T. Soane, R. Layfield, P.W. Sheppard, T. Ebendal, D. Usoskin, J. Lowe, and R.J. Mayer. 2008. Depletion of 26S Proteasomes in Mouse Brain Neurons Causes Neurodegeneration and Lewy-Like Inclusions Resembling Human Pale Bodies. J. Neurosci. 28: 8189–8198.

7. Giasson, B.I., and V.M.-Y. Lee. 2003. Are Ubiquitination Pathways Central to Parkinson's Disease? Cell. 114: 1–8.

8. Glickman, M.H., and A. Ciechanover. 2002. The Ubiquitin-Proteasome Proteolytic Pathway: Destruction for the Sake of Construction. Physiol. Rev. 82: 373–428.

9. Welchman, R.L., C. Gordon, and R.J. Mayer. 2005. Ubiquitin and ubiquitin-like proteins as multifunctional signals. Nat. Rev. Mol. Cell Biol. 6: 599–609.

10. Yi, J.J., and M.D. Ehlers. 2007. Emerging Roles for Ubiquitin and Protein Degradation in Neuronal Function. Pharmacol. Rev. 59: 14–39.

11. Saggu, R., T. Schumacher, F. Gerich, C. Rakers, K. Tai, A. Delekate, and G.C. Petzold. 2016. Astroglial NF-kB contributes to white matter damage and cognitive impairment in a mouse model of vascular dementia. Acta Neuropathol. Commun. : 1–10.

12. Subash C Gupta, Chitra Sundaram, Simone Reuter, and B.B.A. 2011. Inhibiting NF-κB Activation by Small Molecules As a Therapeutic Strategy. 1799: 775–787.

13. Hsiao, H., Y. Chen, H. Chen, P. Tu, and Y. Chern. 2018. A critical role of astrocyte-mediated nuclear factor- k B-dependent inflammation in Huntington ' s disease. 22: 1826–1842.

14. Severine, B., C. Vande Velde, and Don W. Cleveland. 2006. ALS : A Disease of Motor Neurons and Their Nonneuronal Neighbors. Neuron. 52: 39–59.

15. Kimelberg, H.K., and M. Nedergaard. 2010. Functions of Astrocytes and their Potential As Therapeutic Targets. 7: 338–353.

16. Dringen, R., J.M. Gutterer, and J. Hirrlinger. 2000. Glutathione metabolism in brain metabolic interaction between astrocytes and neurons in the defense against reactive oxygen species. Eur J Biochem. 267: 4912–4916.

17. Johnson, W.M., A.L. Wilson-Delfosse, and J.J. Mieyal. 2012. Dysregulation of glutathione homeostasis in neurodegenerative diseases. Nutrients. 4: 1399–1440.

18. Aoyama, K., and T. Nakaki. 2013. Impaired glutathione synthesis in neurodegeneration. Int. J. Mol. Sci. 14: 21021–21044.

19. Bernardinelli, Y., D. Muller, and I. Nikonenko. 2014. Astrocyte-Synapse Structural Plasticity. 2014.

20. Rothstein, J.D., M. Dykes-Hoberg, C.A. Pardo, L.A. Bristol, L. Jin, R.W. Kuncl, Y. Kanai, M.A. Hediger, Y. Wang, J.P. Schielke, and D.F. Welty. 1996. Knockout of glutamate transporters reveals a major role for astroglial transport in excitotoxicity and clearance of glutamate. Neuron. 16: 675–686.

21. Storck, T., S. Schulte, K. Hofmann, and W. Stoffel. 1992. Structure, expression, and functional analysis of a Na(+)-dependent glutamate/aspartate transporter from rat brain.

Proc. Natl. Acad. Sci. U. S. A. 89: 10955–9.

22. Lehre, K.P., L.M. Levy, O.P. Ottersen, J. Storm-Mathisen, and N.C. Danbolt. 1995. Differential expression of two glial glutamate transporters in the rat brain: quantitative and immunocytochemical observations. J. Neurosci. 15: 1835–1853.

23. Sidoryk-Wegrzynowicz, M., M. Wegrzynowicz, E. Lee, A.B. Bowman, and M. Aschner. 2011. Role of Astrocytes in Brain Function and Disease. Toxicol. Pathol. 39: 115–123.

24. Gordon, S., and P.R. Taylor. 2005. Monocyte and macrophage heterogeneity. Nat. Rev. Immunol. 5: 953–64.

25. Varol, C., A. Mildner, and S. Jung. 2015. Macrophages: development and tissue specialization. Annu. Rev. Immunol. 33: 643–75.

26. Trang, T., S. Beggs, and M.W. Salter. 2011. Brain-Derived Neurothrophic Factor from glia: A Molecular substrate for neuropathic pain. Neuron Glia Biol. 7: 99–108.

27. Ransohoff, R.M., and A.E. Cardona. 2010. The myeloid cells of the central nervous system parenchyma. Nature. 468: 253–62.

28. Peterson, L.J., and P.M. Flood. 2012. Oxidative stress and microglial cells in Parkinson's disease. Mediators Inflamm. 2012.

29. Frost, J.L., and D.P. Schafer. 2016. Microglia: Architects of the Developing Nervous System. Trends Cell Biol. 26: 587–597.

30. Paolicelli, R.C., G. Bolasco, F. Pagani, L. Maggi, M. Scianni, P. Panzanelli, M. Giustetto, T.A. Ferreira, E. Guiducci, L. Dumas, D. Ragozzino, and C.T. Gross. 2011. Synaptic pruning by microglia is necessary for normal brain development. Science. 333: 1456–8.

31. Bialas, A.R., and B. Stevens. 2013. TGF-Beta Signaling Regulates Neuronal C1q Expression and Developmental Syanptic Refinement. Nat. Neurosci. 16: 1773–1782.

32. Roumier, A. 2004. Impaired Synaptic Function in the Microglial KARAP/DAP12-Deficient Mouse. J. Neurosci. 24: 11421–11428.

33. Lee, M. 2013. Neurotransmitters and microglial-mediated neuroinflammation. Curr. Protein Pept. Sci. 14: 21–32.

34. Pannell, M., F. Szulzewsky, V. Matyash, S.A. Wolf, and H. Kettenmann. 2014. The subpopulation of microglia sensitive to neurotransmitters/neurohormones is modulated by stimulation with LPS, interferon- Y, and IL-4. Glia. 62: 667–679.

35. Colonna, M., and O. Butovsky. 2017. Microglia Function in the Central Nervous System During Health and Neurodegeneration. Annu. Rev. Immunol. 35: 441–468.

36. Sofroniew, M. V. 2015. Astrogliosis. : 1–16.

37. Frank-cannon, T.C., L.T. Alto, F.E. Mcalpine, and M.G. Tansey. 2009. Does neuroinflammation fan the flame in neurodegenerative diseases ? 13: 1–13.

38. Kawai, T., and S. Akira. 2007. Signaling to NF- k B by Toll-like receptors. 13.

39. Hamby, M.E., G. Coppola, Y. Ao, D.H. Geschwind, B.S. Khakh, and M. V Sofroniew. 2012. Inflammatory Mediators Alter the Astrocyte Transcriptome and Calcium Signaling Elicited by Multiple G-Protein-Coupled Receptors. J. Neurosci. 32: 14489–14510.

40. Lee, J.H., W.H. Yu, A. Kumar, S. Lee, P.S. Mohan, C.M. Peterhoff, D.M. Wolfe, M. Martinez-Vicente, A.C. Massey, G. Sovak, Y. Uchiyama, D. Westaway, A.M. Cuervo, and R.A. Nixon. 2010. Lysosomal proteolysis and autophagy require presenilin 1 and are disrupted by Alzheimer-related PS1 mutations. Cell. 141: 1146–1158.

41. Yu, H.-M., Y.-M. Zhao, X.-G. Luo, Y. Feng, Y. Ren, H. Shang, Z.-Y. He, X.-M. Luo, S.-D. Chen, and X.-Y. Wang. 2012. Repeated Lipopolysaccharide Stimulation Induces Cellular Senescence in BV2 Cells. Neuroimmunomodulation. 19: 131–136.

42. Bosma-Den Boer, M.M., M.L. Van Wetten, and L. Pruimboom. 2012. Chronic inflammatory diseases are stimulated by current lifestyle: How diet, stress levels and medication prevent our body from recovering. Nutr. Metab. 9: 1–14.

43. Peng, J., F.F. Stevenson, M.L. Oo, and J.K. Andersen. 2009. Iron-enhanced paraquat-mediated dopaminergic cell death due to increased oxidative stress as a consequence of microglial activation. Free Radic. Biol. Med. 46: 312–320.

44. Litteljohn, D., E. Mangano, M. Clarke, J. Bobyn, K. Moloney, and S. Hayley. 2011. Inflammatory Mechanisms of Neurodegeneration in Toxin-Based Models of Parkinson's Disease. Parkinsons. Dis. 2011: 1–18.

45. Morales, I., L. Guzmán-martínez, C. Cerda-troncoso, G.A. Farías, and R.B. Maccioni. 2014. Neuroinflammation in the pathogenesis of Alzheimer ' s disease . A rational framework for the search of novel therapeutic approaches. 8: 1–9.

46. Ciechanover, A. 2005. Intracellular protein degradation: from a vague idea thru the lysosome and the ubiquitin–proteasome system and onto human diseases and drug targetingNobel Lecture 2004, © The Nobel Foundation 2004. Cell Death Differ. 12: 1178–1190.

47. Jürgen Dohmen, R. 2004. SUMO protein modification. Biochim. Biophys. Acta - Mol. Cell Res. 1695: 113–131.

48. Müller, S., C. Hoege, G. Pyrowolakis, and S. Jentsch. 2001. Sumo, ubiquitin's mysterious cousin. Nat. Rev. Mol. Cell Biol. 2: 202–210.

49. Ulrich, H.D. 2005. Mutual interactions between the SUMO and ubiquitin systems: A plea of no contest. Trends Cell Biol. 15: 525–532.

50. Desterro, J.M.., M.S. Rodriguez, and R.T. Hay. 1998. SUMO-1 Modification of IκBα Inhibits NF-κB Activation. Mol. Cell. 2: 233–239.

51. Huang, Q., and M.E. Figueiredo-Pereira. 2010. Ubiquitin/proteasome pathway impairment in neurodegeneration: Therapeutic implications. .

52. Choi, S.S., H.J. Lee, I. Lim, J.I. Satoh, and S.U. Kim. 2014. Human astrocytes: Secretome profiles of cytokines and chemokines. PLoS One. 9.

53. Mémet, S. 2006. NF-κB functions in the nervous system: From development to disease. Biochem. Pharmacol. 72: 1180–1195.

54. Medeiros, R., and F.M. Laferla. 2013. Astrocytes : Conductors of the Alzheimer disease neuroin fl ammatory symphony. Exp. Neurol. 239: 133–138.

55. Kaltschmidt, B., and C. Kaltschmidt. 2009. NF- k B in the Nervous System. .

56. Kaltschmidt, C., I.B. Kaltschmidt, H. Neumann, H. Wekerle, and P.A. Baeuerle. 1994. Constitutive NF-KB Activity in Neurons. 14: 3981–3992.

57. Chinta, S.J., C.A. Lieu, M. Demaria, R.M. Laberge, J. Campisi, and J.K. Andersen. 2013. Environmental stress, ageing and glial cell senescence: A novel mechanistic link to parkinson's disease? J. Intern. Med. 273: 429–436.

58. Fernandez-Lizarbe, S., M. Pascual, and C. Guerri. 2009. Critical Role of TLR4 Response in the Activation of Microglia Induced by Ethanol. J. Immunol. 183: 4733–4744.

59. Wang, Z., D. Liu, F. Wang, S. Liu, S. Zhao, E. Ling, and A. Hao. 2019. Saturated fatty acids activate microglia via Toll-like receptor 4 / NF- k B signalling. : 229–241.

60. Kermanian, F., M. Mehdizadeh, M. Soleimani, A.R.E. Bideskan, J. Hami, H. Kheradmand, and H. Haghir. 2014. Adenosine A2a receptors activate Nuclear Factor-Kappa B (NF-κB) in rat hippocampus after exposure to different doses of MDMA. Mol. Cell. Toxicol. 10: 59–66.

61. Oeckinghaus, A., and S. Ghosh. 2009. The NF-kB Family of Transcription Factors and Its Regulation. Cold Spring Harb Perspect Biol. : 1–15.

62. Carrero, I., M.R. Gonzalo, B. Martin, J.M. Sanz-Anquela, J. Arévalo-Serrano, and A. Gonzalo-Ruiz. 2012. Oligomers of beta-amyloid protein (Aβ1-42) induce the activation of cyclooxygenase-2 in astrocytes via an interaction with interleukin-1beta, tumour necrosis factor-alpha, and a nuclear factor kappa-B mechanism in the rat brain. Exp. Neurol. 236: 215–227.

63. Garwood, C.J., J.D. Cooper, D.P. Hanger, and W. Noble. 2010. Anti-inflammatory impact of minocycline in a mouse model of tauopathy. Front. Psychiatry. 1: 1–8.

64. Song, Z.P., B.R. Xiong, X.H. Guan, F. Cao, A. Manyande, Y.Q. Zhou, H. Zheng, and Y.K. Tian. 2016. Minocycline attenuates bone cancer pain in rats by inhibiting NF-κB in spinal astrocytes. Acta Pharmacol. Sin. 37: 753–762.

65. Yu, L., C. Chen, L.F. Wang, X. Kuang, K. Liu, H. Zhang, and J.R. Du. 2013. Neuroprotective Effect of Kaempferol Glycosides against Brain Injury and Neuroinflammation by Inhibiting the Activation of NF-κB and STAT3 in Transient Focal Stroke. PLoS One. 8.

66. Lawrence T. 2009. The nuclear factor NF-kappaB pathway in inflammation. Cold Spring Harb. Perspect. Biol. 1: 1–10.

67. Huang, W.C., J.J. Chen, H. Inoue, and C.C. Chen. 2003. Tyrosine Phosphorylation of I-_k_B Kinase ⁄ by Protein Kinase C-Dependent c-Src Activation Is Involved in TNF--Induced Cyclooxygenase-2 Expression. J. Immunol. 170: 4767.

68. Collins, P., I. Mitxitorena, and R. Carmody. 2016. The Ubiquitination of NF-κB Subunits in the Control of Transcription. Cells. 5: 23.

69. Huxford, T., and G. Ghosh. 2009. A Structural Guide to Proteins of the NF- k B. : 1–17.

70. Gilmore, T.D. 2006. Introduction to NF- j B : players , pathways , perspectives. : 6680–6684.

71. Kaltschmidt, B., D. Widera, and C. Kaltschmidt. 2005. Signaling via NF- n B in the nervous system. 1745: 287–299.

72. Israe, A. 2010. The IKK Complex , a Central Regulator of NF- k B Activation. : 1–14.

73. Karin, M. 1999. How NF- k B is activated : the role of the I k B kinase (IKK) complex. Mol. Cell. Biol. 16: 1295–1304.

74. Rushe, M., L. Silvian, S. Bixler, L.L. Chen, A. Cheung, S. Bowes, H. Cuervo, S. Berkowitz, T. Zheng, K. Guckian, M. Pellegrini, and A. Lugovskoy. 2008. Structure of a NEMO / IKK-Associating Domain Reveals Architecture of the Interaction Site. : 798–808.

75. Xu, G., Y. Lo, Q. Li, G. Napolitano, and X. Wu. 2011. Crystal structure of inhibitor of κB kinase β (IKKβ). 472: 325–330.

76. Siggers, T., A.B. Chang, A. Teixeira, D. Wong, K.J. Williams, B. Ahmed, J. Ragoussis, I.A. Udalova, S.T. Smale, and L. Martha. 2012. Principles of dimer-specific gene regulation revealed by a comprehensive characterization of NF-κB family DNA binding. 13: 95–102.

77. May, M.J., S.E. Larsen, J.H. Shim, L.A. Madge, and S. Ghosh. 2004. A Novel Ubiquitin-like Domain in IKKb Kinase Is Required for Functional Activity of the Kinase. 279: 45528–45539.

78. Ramana, C. V, M. Chatterjee-kishore, H. Nguyen, and G.R. Stark. 2000. Complex roles of Stat1 in regulating gene expression. 1.

79. Mitchell, T.J., and S. John. 2005. Signal transducer and activator of transcription (STAT) signalling and T-cell lymphomas. Immunology. 114: 301–12.

80. Majoros, A., E. Platanitis, E. Kernbauer-Hölzl, F. Rosebrock, M. Müller, and T.

Decker. 2017. Canonical and non-canonical aspects of JAK-STAT signaling: Lessons from interferons for cytokine responses. Front. Immunol. 8.

81. Bhattacharya, S., and C. Schindler. 2003. Regulation of Stat3 nuclear export. J. Clin. Invest. 111: 553–559.

82. Ferrao, R., and P.J. Lupardus. 2017. The Janus Kinase (JAK) FERM and SH2 domains: Bringing specificity to JAK-receptor interactions. Front. Endocrinol. (Lausanne). 8: 1–11.

83. Mcbride, K.M., G. Banninger, C. Mcdonald, and N.C. Reich. 2002. Regulated nuclear import of the STAT1 transcription factor by direct binding of importin- a. 21.

84. Reich, N.C. 2007. STAT dynamics. Cytokine Growth Factor Rev. 18: 511–518.

85. Böhmer, F.-D., and K. Friedrich. 2014. Protein tyrosine phosphatases as wardens of STAT signaling. Jak-Stat. 3: e28087.

86. Krebs, D.L., and D.J. Hilton. 2001. SOCS proteins: negative regulators of cytokine signaling. Stem Cells. 19: 378–87.

87. Qin, H., S.A. Niyongere, S.J. Lee, B.J. Baker, and E.N. Benveniste. 2008. Expression and functional significance of SOCS-1 and SOCS-3 in astrocytes. J. Immunol. 181: 3167–76.

88. Ungureanu, D., P. Saharinen, I. Junttila, D.J. Hilton, and O. Silvennoinen. 2002. Regulation of Jak2 through the ubiquitin-proteasome pathway involves phosphorylation of Jak2 on Y1007 and interaction with SOCS-1. Mol. Cell. Biol. 22: 3316–26.

89. Morales, J.K., Y.T. Falanga, A. Depcrynski, J. Fernando, and J.J. Ryan. 2010. Mast cell homeostasis and the JAK-STAT pathway. Genes Immun. 11: 599–608.

90. H, O. 2016. A phosphorylation-acetylation switch regulates STAT1 signaling. : 223–235.

91. Currais, A., W. Fischer, P. Maher, and D. Schubert. Intraneuronal protein aggregation as a trigger for inflammation and neurodegeneration in the aging brain. 31: 5–10.

Abbreviations.

- Sodium dodecyl sulphate polyacrylamide-gel electrophoresis (SDS-PAGE)
- 2-Acrylamido-2-methyl-1-propanesulfonic acid (AMPS)
- Tetramethylethylenediamine (TEMED)
- Neurodegenerative disorders (ND's).
- Amyotrophic lateral sclerosis (ALS).
- Alzheimer's disease (AD).
- Multiple sclerosis, (MS).
- The Janus kinase/signal transducer and activator of transcription 3 (JAK/STAT3).
- Mitogen-Activated Protein Kinase (MAPK).
- Nuclear Factor kappa-light-chain-enhancer of activated B cells (NF-κB).
- Nuclear factor of kappa light polypeptide gene enhancer in B-cells inhibitor, alpha (IκBα).
- The Ubiquitin Proteasome Pathway (UPP).
- The central / peripheral nervous system (CNS / PNS).
- Glutathione (GSH).
- Fibroblast growth factors (FGF).
- Nerve growth factor (NGF).
- Insulin like growth factor 1 (IGF-1).
- G-aminobutyric acid (GABA).
- Glutamate aspartate transporter (GLAST).
- Neuron growth factor (NGF).
- Brain derived Neuron Factor (BDNF).
- Fibroblast Growth Factor (FGF-2).
- Tricarboxylic acid cycle (TCA cycle).
- Blood-brain barrier (BBB).
- Small ubiquitin-like modifier (SUMO).
- Senescence-associated heterochromatin foci (SAHF).
- Interleukin (IL-1β, IL-6).
- Intracellular Nitric oxidase (iNOS).
- Tumour necrosis factor alpha (TNFα).
- Glial Fibrillary acidic Protein (GFAP).
- Ionized calcium binding adaptor molecule 1 (IBA-1).

Appendix

1. Total homogenate sample preparation- Lawler, K- Dec 2017 & Mohamed, H-Nov 2013.

¼ of the cortex from previously collected samples were homogenised in 500 µl of a protein lysis buffer and protease cocktail inhibitor. This was achieved utilising a ceramic bead system the 'bead beater' which required two rounds of 20 seconds. Immediately after this, centrifuge contents for 10 minutes at 10,000 RPM set to 4 C. The resultant supernatant was aliquoted and stored at – 80 C until further use.

Protein Lysis Buffer	• Tris: 50 mM. • Sodium Chloride: 150 mM. • EDTA: 2 mM. • Magnesium Chloride: 1 mM. • Sodium Fluoride: 100 mM. • Glycerol: 10%. • Triton X-100: 1%. • Sodium deoxycholate: 1%. • SDS: 0.1%. • Sucrose: 125 mM. • Protease Inhibitor Cocktail: 1%.

2. Bradford Assay

Used to measure protein concentration in samples. The binding of Commassie brilliant blue to protein is an advantageous method due to its simplicity and rapidity of results. A colour change of red to blue indicates the presence of protein in the sample (sensitive down to 20 ug per cm^{-3}) in a concentration dependent manner.

- Bovine serum albumin (BSA) 1mg/ml (thawed).
- Add water to 96 plate as illustrated in figure 2.
- Wells must be filled up to 50 (µl) for both samples and replicates.

Prepare Bradford reagent (BR) –

BR $_{(0.5\ mL)}$ + Distilled water 5.5 $_{(mL)}$ = Bradford assay solution 6 $_{(mL)}$ **(BAS)**

5. Pipette 150 $_{(µl)}$ BAS into each well containing samples and replicates of the 96 plate assay.

Figure: Representation of 96 plate BSA Bradford Assay

	1	2	3	4
A 0% BSA	**50(µl) (water)**	**50(µl) (water)**	**48W+2S(µl)**	**48W+2S(µl)**
B 5% BSA	**45(µl) (water) + 5(µl) (BSA)**	**45(µl) (water) + 5(µl) (BSA)**		
C 10% BSA	**40(µl) (water) + 10(µl) (BSA)**	**40(µl) (water) + 10(µl) (BSA)**		
D 15% BSA	**35(µl) (water) + 15(µl) (BSA)**	**35(µl) (water) + 15(µl) (BSA)**		
E 20% BSA	**30(µl) (water) + 20(µl) (BSA)**	**30(µl) (water) + 20(µl) (BSA)**		
F 30% BSA	**20(µl) (water) + 30(µl) (BSA)**	**20(µl) (water) + 30(µl) (BSA)**		
G 40% BSA	**10µl) (water) + 40(µl) (BSA)**	**10µl) (water) + 40(µl) (BSA)**		
H 50% BSA	**50(µl) (BSA)**	**50(µl) (BSA)**		

Bradford Assay Analysis

1. Set the plate reader to 595 $_{(nM)}$ and scan. Record results and input into Excel as a graph.

EXAMPLE: Finding the concentration of your samples:

$$y = 0.0095x + 0.2396$$

Concentration= (y-mx)/c

Or

S1 Absorbance	R1 Absorbance	Average	S2 Absorbance	R2 Absorbance	Average
0.536	0.682	0.609	0.372	0.554	0.463

Thus

Sample	Absorbance	Protein concentration	Average
A3 Mutant Type	**0.536**	**(0.536-0.2396) / (0.0095) = 31.20**	**31.20 + 46.75 / 2 = 38.885**
A4 Mutant Type	0.682	46.57	
A5 Wild Type	0.372	13.94	23.515
A6 Wild Type	0.554	33.09	

Finally, this figure must be divided by the number of (µl) used in the sample-

Mutant Average= 38.885/2 = 19.44 ug in (µl).

Wild Average = 23.515/2 = 11.76 ug in (µl).

3. SDS PAGE Gel cassette preparation.

Reagents needed:

- Resolving Gel Buffer B (1.1 M Tris PH 8.8, 0.1% SDS).
- 0.1% SDS.
- Acrylamide 30%.
- Tetramethylethylenediamine (TEMED).
- Ammonium persulphate 10% (AMPS).
- Stacking Buffer (0.14M Tris Ph 6.8, 0.1% SDS).
- 1L of Electrode Buffer.

Cassette preparation and casting

- Clean Spacer and front plates with 70% Ethanol and dry.
- Assemble in casting frames and lock into place.
- Prepare resolving gel and load.
- Pippete 4.7 ml of resolving gel per preassembled cassette.

Overlay with water saturated butanol.

Reagent	10 / 12% SDS-GEL
0.1% SDS	1.33 / 1.67 ml
Buffer B	1.66 / 1.67 ml
Acrylamide	2.0 / 1.67 ml
AMPS	50 µl
TEMED	5 µl

After the resolving gel has set, remove water saturated butanol layer with deionised water.

Prepare the stacking gel as follows:

Reagent	
Stacking gel buffer	1.56 ml
Acrylamide	0.312 ml
AMPS	37.5 µl
TEMED	7.5 µl

- Load 1ml per cassette.
- Immediately insert and secure well forming comb.
- Leave to polymerise for at least 30 minutes.

4. Immunohistochemistry Staining of Paraffin sections mouse and rabbit primary. (Mouse on Mouse (M.O.M) kit PK-2200) & (Rabbit kit PK-6101) Vectastain Elite ABC kit- Vector Labs Ltd.

Dewax and rehydrate samples as follows (Fume hood):

10 minutes of immersion in each of-

- Xylene.
- 100% Ethanol.
- 95% Ethanol.
- 70% Ethanol.

This is followed by 5 minutes in gently running water. Antigen retrieval follows after rehydration. These two solutions were used, depending upon the required reagents/ procedure.

[PH 6]10mM Sodium Citrate Retrieval Solution, 0.05% Tween:

- 2.35g of Sodium citrate.
- 800ml of dH_2O.
- 400 µl of Tween-20.
- Adjust to PH 6.

Heat slides in solution at 100 °C (approx.) for 20 minutes. Remove from heat and allow to cool for 20 minutes further whilst on a shaker. Remove solution with gently running water for 10 minutes

Endogenous peroxide block- Incubate slides for 10 minutes in 3% H_2O_2 in tap water. Follow this with 5-minute washes in gently running water and PBS whilst on a shaker.

Blocking Non-Specific Background

M.O.M: use M.O.M Ig blocking reagent [36 µl stock solution in 1ml PBS]

Rabbit: use 3% serum-specific block [serum specific to species secondary antibody was raised in].

60 µl is needed per section. Incubate for 1 hour in humid chamber at room temperature.

Wash in PBS 3 times 10-minute washes post incubation.

Primary Antibody

Dilute Ig to appropriate concentration and volume (60µl) in either:

Mouse: M.O.M Diluent.

Rabbit: Same as blocking solution.

Primary Incubation occurs for 1 hour for GFAP (room temperature), and overnight at 4 °C for all other primary Ig's (requires gene frame and 65 µl).

Wash in PBS 3 times 10-minute washes post incubation.

Secondary Antibody

Dilute Ig to appropriate concentration and volume (60µl) in the same manner used to prepare the primary solutions. Incubate for 1 hour in a humid chamber.

Wash in PBS 3 times 10-minute washes post incubation.

Detection: ABC Reagent

Apply ABC reagent as indicated in kit and incubate for 30 minutes.

DAB (Diaminobenzidine) Staining

0.03% DAB Staining Solution:

- 8ml 1 M Tris pH 7.5.
- 72 ml of water (tap).
- 40 µl DAB.

Mix well and use immediately. Incubate until sufficient browning has occurred. To stop the reaction, introduce gently running water for 10 minutes.

Counterstain: Nuclei counter staining

- Incubate slides in Haematoxylin [Harris] for 10 minutes.
- Rinse in water till clear running water appears.
- Dip (15 seconds) in 1 % acid-alcohol (HCL in 70% Ethanol).
- Wash in gently running water for 10 minutes.

Dehydrate and Mount (Fume Hood)

- Dip in 70% Ethanol.
- Dip in 95% Ethanol.
- 30 seconds in 100% Ethanol.
- 45 seconds in Xylene.
- Mount coverslip with DPX.

5. Immunofluorescence, Adapted from ABC Vectastain Kit.

Dewax and rehydrate samples as follows (Fume hood):

10 minutes of immersion in each of-

- Xylene.
- 100% Ethanol.
- 95% Ethanol.
- 70% Ethanol.

This is followed by 5 minutes in gently running water. Antigen retrieval follows after rehydration. These two solutions were used, depending upon the required reagents/ procedure.

[PH 6]10mM Sodium Citrate Retrieval Solution, 0.05% Tween:

- 2.35g of Sodium citrate.
- 800ml of dH_2O.
- 400 µl of Tween-20.
- Adjust to PH 6.

Heat slides in solution at 100 C (approx.) for 20 minutes. Remove from heat and allow to cool for 20 minutes further whilst on a shaker. Remove solution with gently running water for 10 minutes

***Endogenous peroxide block*-** Incubate slides for 10 minutes in 3% H_2O_2 in tap water. Follow this with 5-minute washes in gently running water and PBS whilst on a shaker.

Blocking Non-Specific Background

Fill a large container with ice and put in fume cupboard Prepare sodium borohydride solution just before use:

- 0.15g sodium borohydride in150ml PBS.
- Incubate slides in solution on ice for 3 x 10 mins, using fresh solution each time.

NB – keep the bottle with the remaining sodium borohydride solution on ice while not using.

- Wash 6 x 5min washes in 0.9% saline at room temperature.

This is followed by blocking using the appropriate serum:

M.O.M: use M.O.M Ig blocking reagent [36 µl stock solution in 1ml PBS].

Rabbit: use 3% serum-specific block [serum specific to species secondary antibody was raised in].

60 µl is needed per section. Incubate for 1 hour in humid chamber at room temperature.

Wash in PBS 3 times 10-minute washes post incubation.

Primary Antibody

Dilute Ig to appropriate concentration and volume (60µl) in either:

Mouse: M.O.M Diluent.

Rabbit: Same as blocking solution.

Primary Incubation occurs for 1 hour for GFAP (room temperature), and overnight at 4 C for all other primary Ig's (requires gene frame and 65 µl).

Wash in PBS 3 times 10-minute washes post incubation.

Secondary Antibody

Dilute Ig to appropriate concentration and volume (60µl) in the same manner used to prepare the primary solutions. Incubate for 1 hour in a ***dark*** humid chamber.

Wash in PBS 3 times 10-minute washes post incubation.

6. Dual Immunofluorescent Staining.

- Re block for 30 mins using serum appropriate to the second primary antibody.
- Continue as previously described for primary antibody and secondary antibody steps

NB – ensure you use different colours for different proteins, and ensure your fluorescent

Secondary antibody is appropriate for your primary.

Counterstain: Nuclei counter staining

- Dilute DAPI (stock is 5mg/ml) into a 1:1000 dilution in PBS.
- Apply DAPI stain and incubate in dark humid chamber for 5 mins room temperature.
- Wash in PBS 3 times 5 minutes.
- Post fix sections in 4% PFA in PBS for 12 minutes.
- Wash in PBS 3 times 10 minutes.

Dehydrate and Mount (Fume Hood)

- Dip in 70% Ethanol.
- Dip in 95% Ethanol.
- 30 seconds in 100% Ethanol.
- 45 seconds in Xylene.
- Mount coverslip with 12 µl Fluorogel.

7. Traditional PCR Protocol.

- Add 500 µL of Lysis Buffer & 25 µL proteinase K.
- Agitate at 55 C for a minimum of 2 hours. Between 2-24 hours is OK.
- Vortex until sample is well mixed.
- Centrifuge at 10000 RPM for 10 minutes (4 C)
- Remove supernatant to a new Eppendorf.

N.B Keep both the supernatant and pellet from all samples.

500 µL is usually enough, however be sure not to disturb the pellet. If this occurs, Re-centrifuge sample.

- Add an equal volume of Isopropanol to the supernatant (Step 5).
- Invert sample 10 times.
- Centrifuge at 13000 RPM for 10 minutes. (Room Temperature)
- Remove supernatant.
- Add 500 µL of 70% Ethanol.
- Centrifuge at 13000 RPM for 10 minutes. (Room Temperature)
- Remove Ethanol.
- Air dry remaining pellet for a minimum of 30 minutes.

Preparing Genomic Sample Solution (gDNA)

Ensure Water used is autoclaved, deionised and filtered.

REMOVE an appropriate amount from stock,

1. Re-suspend pellet (Step 9) in water.

    - Add a minimum of 100 µL to ear tissue samples (120 µL or so).
    - Add a minimum of 350 µL to tail tissue samples.

2. Vortex sample gently.
3. Leave sample for a minimum of 15 minutes. During this time, Prepare PCR master mix (See below).

N.B Ensure the reagents are appropriately de-frozen and mixed.

Cre Recombinase Master Mix per sample

Reagent	Volume (µL)	41 x Volume (µL)
dNTPS	1.0	41
10 x Taq PCR buffer	1.0	41
Sense Cre primer	0.5	22
Anti-Sense Cre Primer	0.5	22
Taq Polymerase	0.05	2.2
Water	Total 9.5 µL	261.3

Psmc1 (26S proteasome AAA-ATPase) Master Mix <u>per sample</u>

Reagent	Volume (µL)	41 x Volume (µL)
dNTPS	1.0	41
10 x Taq PCR buffer	1.0	41
D1360 Primer	0.5	22
LB3 Primer	0.5	22
X316 Primer	0.5	22
Taq Polymerase	0.05	2.2
Water	Total 9.5 µL	239.3

Loading PCR Plate

- Load Master Mix for both samples 9.5 µL to each Well. Due to the need for DNA Ladders and Controls, 92 wells are available to use (See below)
- Add 0.5 µL of gDNA (Step 3) to each well.
- Close PCR Lids

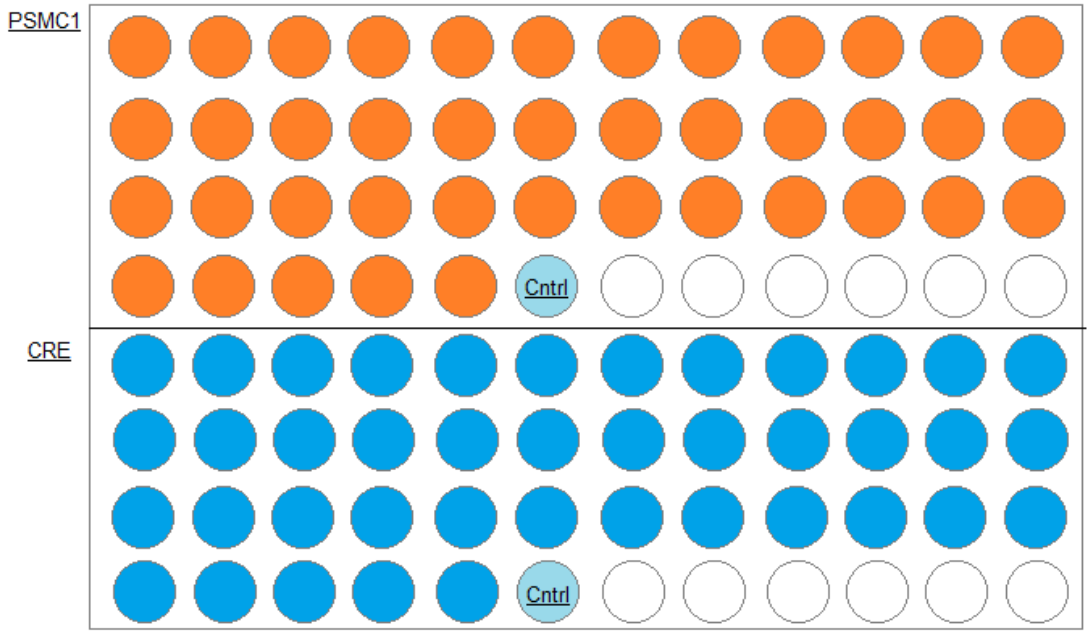

8. Agarose Gel Preparation

- Prepare TAE Buffer

TAE 50 X	20 mL
Distilled Water.	980 mL

- Prepare 3% Running Gel

TAE Buffer	150 mL
Agarose (Fine)	4.5 g

- Heat for 7 minutes setting: Defrost in microwave.

N.B The viscosity of the solution should be such that no lumps are left. The desired viscosity should be more akin to water than oil. Furthermore, there should be no residual solution on the walls of the flask when swirled.

The solution requires extreme caution- the temperature required increases the possibility of the solution 'fizzing' up and out of the flask.

- Set the Gel Tank up appropriately.
- Add 7.5 µL of ethidium bromide and swirl gently.
- Pour gel steadily in one corner area.
- Allow to set for 30 minutes.

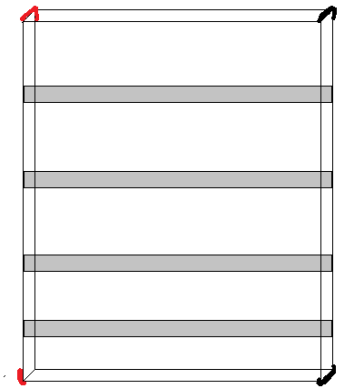

Pipetting PCR samples

1. Pour TAE Buffer to Max Line.
2. Pippete 3 µL of DNA ladder into the preformed wells.

N.B If using 4 rows, Pippete 2 µL ethidium bromide into the TAE Buffer.

This ensures the bands are properly dyed, as the dye runs antiparallel to the DNA samples.

3. Pippete 10 µL of sample into wells.
4. Run at 145 V for 30 minutes.
5. When the dye fronts and DNA Ladder bands have separated, as shown in Figure 2, switch the Power Supply Unit off.

Figure 2 Finished Agarose Gel at 145 V and 3µL of DNA Ladder

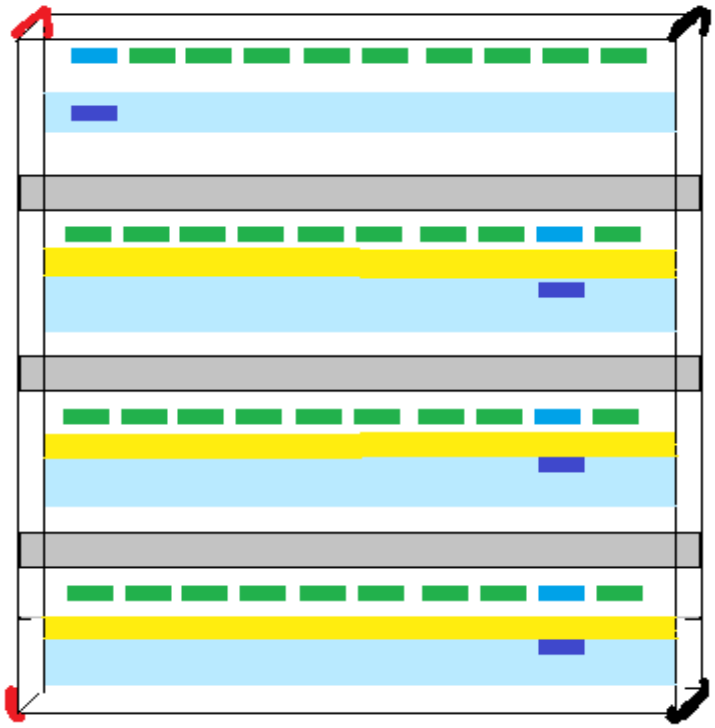

Imaging of Gel

N.B Wear gloves at all time when handling gel due to toxicity.

1. Open SnapGene.
2. Position Gel as appropriate, adjust using control panel of SnapGene, which records in real time.
3. Take picture.

9. Crude Nuclear Extraction Protocol

- Prepare buffered sucrose solution (Table 1) and place on ice until ready to use.
- Homogenise ¼ cortices (50 µg approx.). With a Dounce tissue grinder in 400 µl of ice-cold buffered sucrose solution (IBSS).
- Place Tissue into Homogeniser.
- Homogenise Tissue- Perform 10 down strokes, slowly but firmly- there should be no sound produced, otherwise too much pressure is being used.

This is the <u>Total Homogenate</u>. Separate 50 µl into a labelled tube.

<u>N.B ENSURE THAT IBBS IS ALWAYS ICE-COLD.</u>

<u>ADD 1%</u> (v/v) protease inhibitor cocktail <u>JUST BEFORE USE</u>.

(5 µl for 500 µl)

Formation of Nuclear Fraction.

- Centrifuge Total Homogenate for (10 minutes) at 500 g.
- Remove supernatant **(KEEP)** and re-suspend the remaining pellet in 200 µl of IBSS.
- Centrifuge for (10 minutes) at 1000 g.
- Remove supernatant **(KEEP), combining with the previous from step 5;** leaving the **<u>Nuclear Rich Pellet</u>**.
- Re-suspend Nuclear Rich Pellet in 200 µl of IBSS.

Formation of Cytosolic Fraction.

- Centrifuge for (10 minutes) at 7000 g.
- The **SUPERNATANT** from this process is the **<u>Cytosolic Fraction.</u>**

Formation of Mitochondrial Fraction

- Re-suspend the pellet obtained from the Cytosolic Fraction in 200 µl of IBBS.
- Centrifuge for 600 seconds (10 minutes) at 7000 g.
- Remove supernatant **(DISCARD)** and re-suspend remaining pellet in 100 µl of IBBS.

Table 1: Buffered Sucrose Solution (IBSS)

Reagent	Molecular Mass (g)	Concentration (M)	Weight (g) for Required concentration (1L)	Weight (g) in (10 mL)
HEPES	238.3012	0.002	0.4766024	0.004766025
Mannitol	182.172	0.21	38.25612612	0.38256126
Sucrose	342.2965	0.07	23.96075548	0.239607555
EDTA	292.24	0.0001	0.029224	0.00029224

10. General Solutions used in study (produced in-house)

Solution.	**Reagents and Measurements.**
Western Transfer Buffer.	• Tris: 9.0 [g]. • Glycine: 42.0 [g]. • Methanol: 600 [ml]. • D H_2O: make up to 3000 [ml].
Electrode Buffer.	• Tris: 3.0 [g]. • Glycine: 14.0 [g]. • SDS: 1.0 [g]. • D H_2O: make up to 1000 [ml].
Tris-Buffered Saline Tween (TBST).	• Tris: 2.4 [g]. • Sodium Chloride: 17.5 [g]. **CALLIBRATE pH TO 7.5 (HCl).** • D H_2O: make up to 2000 [ml].
Phosphate-Buffered Saline (PBS)	• Di-Sodium Hydrogen Orthophosphate: 2.84 [g]. • Sodium Chloride: 17.5 [g].
0.1% Sodium Dodecyl Sulphate (SDS).	• SDS: 0.2 [g]. • D H_2O: make up to 200 [ml]. **CALLIBRATE pH TO 7.5 (HCl).** • D H_2O: make up to 2000 [ml].

Buffer B	• Tris: 26.65 [g]. • SDS: 0.2 [g]. **CALLIBRATE pH TO 7.5 (HCl).** • D H_2O: make up to 200 [ml].
Bradford Reagent	• Commassie Blue Brilliant (G2): 100.0 [mg]. • Ethanol: 50.0 [ml]. • Perchloric Acid: 100.0 [ml]. • D H_2O: 50.0 [ml].

11.. Reagent Suppliers

Reagent	**Supplier**	**Code**
Agarose	SeaKem	50004
D-Mannitol	Fisher Scientific	BP686-500
Tris-sodium citrate dihydrate	Fisher Scientific	S/3320/53
Tris	Fisher Scientific	BP121-1
Triton X-100	Sigma-Aldrich	X100-500ml
Glycine	Sigma-Aldrich	G8898-1KG
Sodium Chloride	Fisher Scientific	S/3120/63
Commassie Blue Brilliant (G2)	Sigma-Aldrich	B11-31
Ammonium Persulphate	Sigma-Aldrich	A3678-100G
Perchloric Acid		
Sodium Dodecyl Sulphate (SDS)	Fisher Scientific	BP166-500
Bovine Serum Albumin (BSA)	Fisher Scientific	BP1600-100
Skimmed Dehydrated Milk Powder	Marvel	NA
EDTA	NA	NA
HEPES	NA	NA
Maltose	Sigma-Aldrich	M5885
Sucrose	Fisher Scientific	S/8600/60
Protease Inhibitor Cocktail		
Paraformaldehyde	Fisher Scientific	P084053
Xylene	Fisher Scientific	X0250PB17
Ethanol	Fisher Scientific	E/0650DFC17
Methanol	VWR International	67-65-1
Copper phthalocyanine-3,4′,4″,4‴-tetrasulfonic acid tetrasodium salt	Sigma-Aldrich	NA

12.. Statistical Analysis

GFAP Percentage calculation from fluorescent imaging / co-localisation.

- Open *ImageJ*.
- Select desired image and convert the .Tiff File to 16-bit image.
- Duplicate 16-bit image.
- Create Binary Mask.

A binary mask serves isolates the areas of the brightest fluorescence and assigns them a value of 1. The rest of the image is given the value 0, allowing the expression of the brightest areas as a percentage of the total image.

- Adjust the threshold for whatever is appropriate the sample to eliminate as much background as possible.
- Go to Analyse>Set Measurements.
- Under 'Redirect to', select the 16 bit image.

The Results are then observed, allowing a comparison between samples for further analysis (EXCEL).

t-Test: Two-Sample Assuming Unequal Variances	All samples	All samples	12/12/2018	12/12/2018	15/11/2018	15/11/2018
Results	*WT*	*KO*	*WT*	*KO*	*WT*	*KO*
Mean	**4.669**	**5.449**	**7.702**	**8.404**	**1.876**	**1.509**
Variance	**8.862**	**13.654**	**0.27**	**0.104**	**0.00019**	**0.0565**
Observations	**9**	**7**	4	4	3	3
Hypothesized Mean Difference	0		0		0	
Degrees of Freedom	11		5		2	
t Stat	-0.455062179		-2.291932831		2.667798127	
P(T<=t) one-tail	**0.329**		**0.035**		**0.058**	
P(T<=t) two-tail	**0.658**		**0.07**		**0.116**	

$$T = \frac{\bar{x}_1 - \bar{x}_2}{\sqrt{\frac{s_1^2}{N_1}\frac{+s_2^2}{N_2}}} \qquad \nu \approx \frac{\left(\frac{s_1^2}{N_1} + \frac{s_2^2}{N_2}\right)^2}{\frac{s_1^4}{N_1^2\nu_1} + \frac{s_2^4}{N_2^2\nu_2}}$$

$\bar{x}_=$ Sample mean. $\nu_n \approx N - 1$

$s_=^2$ Sample variance.

$N_=$ Sample size.

T= Welch's T test V= Degree of Freedom